Polymer Chemistry

Macromolecular architectural effects on solution self-assembly of amphiphilic AB-type block copolymers

Journal:	*Polymer Chemistry*
Manuscript ID	PY-REV-11-2023-001324.R1
Article Type:	Review Article
Date Submitted by the Author:	05-Jan-2024
Complete List of Authors:	Ozawa, Naoki; Shinshu Daigaku Nishimura, Tomoki; Shinshu Daigaku, Department of Chemistry and Materials, Faculty of Textile Science and Technology

ARTICLE

Macromolecular architectural effects on solution self-assembly of amphiphilic AB-type block copolymers

Received 00th January 20xx,
Accepted 00th January 20xx

DOI: 10.1039/x0xx00000x

Naoki Ozawa, and Tomoki Nishimura*

Polymers with different architectures, such as block, graft, star, and cyclic polymers, have been developed owing to recent advances in synthetic technology. Notably, minor changes in the architecture of amphiphilic polymers can lead to different self-assembly behaviors, even when their molecular weights and hydrophilic-hydrophobic compositions are similar. This variation in the self-assembly behavior directly affects the properties and performance of self-assembled polymer-based materials. However, a clear understanding of how changes in polymer architecture influence self-assembly behavior is still emerging. This review aims to compare the self-assembly behaviors of amphiphilic AB-type block copolymers with different molecular architectures and elucidate how different polymer architectures influence self-assembly behaviors, as well as their underlying mechanisms. The discussion extends to recent applications, demonstrating how changes in polymer architecture can influence the performance of polymer assemblies used as carriers in drug delivery systems.

1. Introduction

Polymers have a wide variety of architectures, which impart unique physicochemical properties,[1, 2, 3, 4, 5] and these intrinsic structural properties have enabled their widespread application in various biological systems and industries.[6, 7, 8, 9, 10] Natural polymers, such as nucleic acids, proteins, and polysaccharides, possess a variety of structures, including branched structures, cyclic structures, and repeated sequences. Meanwhile, in the field of synthetic polymers, advances in polymerization techniques have provided a diverse array of polymer architectures, including multiblock, graft, star, and cyclic polymers.[4, 11, 12, 13]

Polymer architecture is intrinsically linked to polymer properties and functionalities. Consequently, extensive research has been devoted to investigating the properties of polymers with different structures, in both the bulk and solution phases, to discern the relationships between their structural features and their inherent properties and behaviors.[14, 15, 16, 17, 18] One of the prominent research directions is the self-assembly of amphiphilic polymers in aqueous solutions.[19, 20, 21] The polymer architectures influence the critical micelle concentration (CMC), morphology, and size of the molecular assemblies, as well as their thermoresponsive behavior.[22, 23, 24, 25] In particular, the shape and size of the molecular assemblies dictate the overall properties of the assemblies, requiring careful design and strategic manipulation for their proper application.[26, 27, 28] Thus, a detailed understanding is required for precise engineering of polymer architectures to tailor the properties and performance of amphiphilic polymer assemblies in solution.

The self-assembled structures of amphiphilic polymers are governed by the packing parameter rule, which determines the geometric configurations of molecules within assemblies.[29] Consequently, structural control in the self-assembly of AB-type block polymers can be achieved by manipulating the lengths of the hydrophobic and hydrophilic chains. However, it is not clear whether the self-assembly principles established for AB-type block polymers can be universally applied to polymers with more intricate architectures. For example, it is necessary to compare the properties of molecular assemblies derived from unique polymer structures with those assembled from conventional AB-type polymers. Such information is invaluable for the design and application of self-assembling materials constructed from non-AB-type copolymers.

This review summarizes existing research to elucidate how polymer architectures influence the properties and self-assembly of amphiphilic molecules in solution. Several reviews summarize the self-assembly behavior of linear and nonlinear polymers, but few compare the self-assembly behavior of linear and nonlinear polymers and summarize the effects of structural differences on the self-assembly behavior.[20, 30, 31, 32] We intend to address the findings in this area and then discuss future research directions to provide new guidelines for structural design in polymer science. Specifically, we aim to elucidate the influence of variations in polymer architectures, both linear and nonlinear, on their self-assembly behavior. First, we outline the prevalent synthetic strategies used to prepare linear, cyclic, and star polymers. Our discussion primarily revolves around a diverse array of amphiphilic AB-type copolymers, such as linear diblock and triblock polymers, cyclic block polymers, tadpole polymers, cyclic graft polymers, and star block and miktoarm star polymers (**Fig. 1**). Emphasizing the comparative approach,

Department of Chemistry and Materials Science, Shinshu University, 3-15-1, Tokida, Ueda, Nagano 386-8567, Japan.
E-mail: nishimura_tomoki@shinshu-u.ac.jp

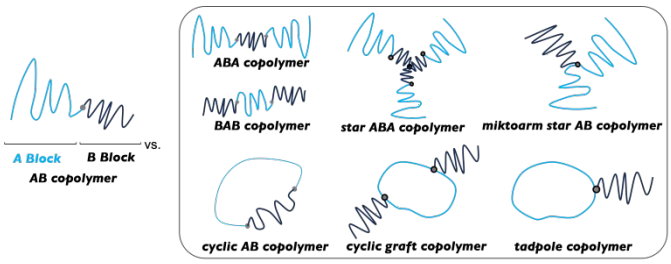

Fig. 1 Illustrations of AB-type block copolymers with different macromolecular architectures featured in this review.

we consider how polymers with identical compositions but different macromolecular architectures exhibit disparate self-assembly properties. Particularly, we examine the underlying factors and thermodynamic or geometric contributions that control the self-assembly behaviors because of variations in the molecular architectures. There are numerous reports describing amphiphilic ABC-type copolymers with different polymer architectures,[33, 34, 35, 36] but this is beyond the scope of this review. In the final part, the review focuses on practical implications, highlighting the utility of these polymer assemblies in drug delivery systems. Finally, we summarize the prevailing challenges and envision prospective advances in the field of polymer architecture and self-assembly.

2. Synthetic strategies for amphiphilic copolymers with various polymer architectures

In this section, we introduce the synthetic strategies of amphiphilic polymers, with a special emphasis on their diverse macromolecular architectures. Initially, we discuss the synthesis of linear polymers, including AB, ABA, and BAB types. Then, the discussion shifts to star polymers, where we introduce three common synthesis methods used to prepare $(AB)_n$ star polymers and miktoarm star polymers, highlighting the foundational concepts of each method. Then, the review turns to the synthetic approach of cyclic copolymers, presenting two prevalent preparation methods. For both star and cyclic polymers, we provide a brief analysis of the advantages and disadvantages associated with the synthetic methods.

1-1. Synthetic strategies for the preparation of ABA copolymers

Two predominant methods for the synthesis of linear ABA triblock copolymers are briefly introduced here. The first method involves coupling A or B blocks with AB copolymers.[37, 38, 39] For example, Zang *et al.* obtained MPEO-*b*-PS-*b*-MPEO triblock polymers by employing a click reaction of azido-functionalized monomethoxy poly(ethylene oxide)-*b*-poly(styrene) (MPEO-PS-N_3) with alkyne-functionalized MPEO. The other method involves the use of bifunctional macroinitiators followed by monomer elongation, referred to as the macroinitiator approach, which is considered a one-step process.[40, 41] The former method requires the introduction of reactive functional groups at the ends of the desired polymers to enable coupling. Although this allows for a diverse range of block selections, it also requires the time-consuming removal of unreacted polymers. In contrast to the coupling method, only polymer chains consisting of polymerizable monomers can be obtained using the macroinitiator method.

1-2. Synthetic strategies for the preparation of amphiphilic AB-type star copolymers

This section briefly discusses the synthesis of star polymers, focusing primarily on amphiphilic $(AB)_n$ star polymers and miktoarm star polymers. The $(AB)_n$ star polymers consist of n linear AB diblock polymers that converge at a central branching point, forming a star-like structure. Conversely, the miktoarm star polymers consist of different polymers, either hydrophilic or hydrophobic, radiating from a central branching point. Three different strategies are commonly used in the synthesis of star polymers, namely the core-first approach, the arm-first approach, and the grafting-on approach,[12, 42, 43] which have unique characteristics.

1-2-1. Core-first approach

In the core-first approach, as the name implies, synthesis is initiated at the polymer core, from which polymer chains are propagated by the polymerization of selected monomers. Subsequently, another monomer can be polymerized from the pre-existing arms, making this method particularly suitable for the synthesis of $(AB)_n$-type star polymers.[44, 45] A major advantage of this strategy is its simplicity and effectiveness in isolating pure star polymers from crude reactions, even those containing unreacted monomers, ligands, and catalysts, by precipitation or dialysis. However, this method requires careful monitoring to prevent star-star coupling, especially when controlled radical polymerization is used for arm extension, and avoid bimolecular termination.[46] Moreover, it is difficult to directly characterize the number, molecular weight, and polydispersity of the arms. This method is typically limited to the synthesis of star polymers with 3 to 8 arms,[47, 48] mainly because of the inherent complexity of synthesizing functional cores with orthogonal initiating functional groups, a prerequisite for the synthesis of multiarm polymers.

1-2-2. Arm-first approach

The arm-first approach begins by fabricating linear arms with specified molecular weights and compositions. These arms are then reacted with an appropriately proportioned cross-linker to form star polymers. These polymers have high-molecular-weight cores that are intricately cross-linked by covalent bonding and supramolecular interactions. Notably, the core domains can support many compounds through covalent bonding or non-covalent interactions.[49, 50] A key advantage of this method is the ability to precisely control and independently evaluate functional arms with different compositions and structures.,[51, 52] This also facilitates straightforward characterization of the number of polymer chains.[53] However,

with this method, it is more difficult to control the number of polymer chains than it is with other synthetic methods, and cumbersome purification procedures are required to effectively separate pure star polymers from unreacted linear arms.[54, 55]

1-2-3. Grafting-onto approach

In the grafting-onto approach, arms possessing reactive ends that complement each other are connected to a central core. This core serves as a multifunctional coupling agent, facilitating the formation of a star polymer,[56, 57, 58] and dictates the number of arms, which is directly correlated to the number of functional groups present in the core. Furthermore, the arms of the star polymer are synthesized through controlled polymerization prior to the coupling reaction. This approach is particularly efficient in the synthesis of miktoarm star polymers and offers greater control over the structural properties of the resulting polymers. However, the method presents certain challenges, such as a limited number of arms in the synthesized star polymers. This limitation is due to the steric hindrance encountered during the coupling reaction between the core and the arms, preventing the core from accommodating a wide range of functional groups. In addition, the click reaction, a dominant coupling mechanism used in this method, requires longer reaction times and an excess of prepared arms to achieve optimal coupling efficiency. This, in turn, complicates the purification process by requiring the careful removal of unreacted arms.

1-3. Synthetic strategies for the preparation of amphiphilic copolymers with cyclic structures

The following subsections briefly outline the synthesis routes of cyclic polymers. For the detailed synthesis, please refer to the specific review articles.[59, 60, 61] There are two typical strategies for synthesizing cyclic polymers, namely ring-closure and ring-expansion.

1-3-1. Ring-closure approach

The ring-closure strategy includes three approaches: the bimolecular homologous bifunctional approach, the unimolecular homologous bifunctional approach, and the unimolecular heterologous bifunctional approach. In the bimolecular homologous bifunctional approach, cyclic polymer synthesis is achieved by attaching a homologous terminal polymer to a bifunctional linker. The synthesis unfolds in two steps, beginning with the coupling of polymer end groups to small molecule end groups, followed by intramolecular coupling using a small molecule linker. Despite the simplicity of this method, side reactions are likely to occur, and the reaction requires an exact 1:1 molar ratio and high dilution conditions. Such conditions often complicate the synthesis, delaying reaction rates and making it difficult to obtain high-purity cyclic polymers.[62, 63, 64] In contrast, the unimolecular homologous and heterologous bifunctional approaches overcome these drawbacks and have reduced susceptibility to side reactions and oligomerization. Among these approaches, the unimolecular heterologous bifunctional approach exhibits higher efficiencies in homocoupling reactions and fewer intermolecular coupling events.[65] Notably, atom transfer radical polymerization has been combined with click chemistry using copper-catalyzed azide-alkyne cycloaddition (CuAAC) reactions, which represents a significant advance in cyclic polymer synthesis, promoting the efficient production of cyclic polymers characterized by narrow molecular weight distributions.[66] Valued for its remarkable coupling efficiency and functional group compatibility,[67] CuAAC has revolutionized the synthesis paradigms, supporting a diverse spectrum of cyclic polymers.[68, 69, 70, 71, 72, 73]

1-3-2. Ring-expansion approach

The ring-closing approach explained above is inherently versatile and allows for precise control of molecular weight. However, high dilution conditions are required to avoid unwanted chain coupling reactions, and the synthesis of high-molecular-weight cyclic polymers is challenging. Conversely, the ring-expansion approach exhibits a decreasing probability of chain end convergence owing to the entropy loss associated with increased polymer chain lengths. By employing ring monomers and ring initiators/catalysts, or a combination of both, this technique facilitates the synthesis of cyclic polymers with high molecular weights, often exceeding 100 kDa.[74] As a result, a variety of synthetic methodologies have emerged, including ruthenium-[75] and tungsten-catalyzed[76] ring-expanded metathesis polymerization, organocatalytic[77] and Lewis acid-catalyzed[78] ionic polymer synthesis, and advances in reversible addition-fragmentation chain transfer (RAFT)[79] and nitroxide-mediated radical polymerization.[80]

3. Effects of different macromolecular architectures on solution self-assembly

In this section, we aim to elucidate the influence of different macromolecular architectures on self-assembly behavior. A comparative analysis is performed, focusing primarily on the CMC, aggregation number (N_{agg}), and hydrodynamic diameter (D_h), as well as the morphological properties of the resulting self-assembled structures. These parameters are crucial in determining the applicability of polymer assemblies in various fields. This review compares the self-assembly behavior of amphiphilic polymers with different structures, giving preference to those with matching molecular weights for the hydrophilic and hydrophobic segments, to focus on the effects caused solely by variations in polymer structure.

3-1. Comparison of self-assembly behavior between AB-type block copolymers and ABA- or BAB-type copolymers in aqueous solutions

First, the self-assembly behavior of amphiphilic linear AB, ABA, and BAB polymers is described. Considering that the ABA and BAB polymers are AB polymers with one additional hydrophilic or hydrophobic block, we can identify the effects of the additional hydrophilic or hydrophobic block on the self-assembling behaviors of linear AB copolymers (**Table 1**).

Table 1. The self-assembly behaviors of amphiphilic AB, ABA, and BAB copolymers in aqueous solutions.

macromolecular architecture	polymer	$f_{hydrophilic}$ [a]	hydrodynamic diameter [b] (nm)	N_{agg} [c]	CMC [d] (mg/mL)	morphology	reference
AB	$PEO_{1.7k}$-*b*-$PBO_{0.86k}$	0.66	n.d. [e]	74	n.d.	n.d.	81
ABA	$PEO_{0.92k}$-*b*-$PBO_{0.79k}$-*b*-$PEO_{0.92k}$	0.7	n.d.	24	n.d.	n.d.	
AB	$PEO_{1.8k}$-*b*-$PBO_{0.72k}$	0.71	n.d.	37	n.d.	n.d.	
ABA	$PEO_{0.92k}$-*b*-$PBO_{0.58k}$-*b*-$PEO_{0.92k}$	0.76	n.d.	4	n.d.	n.d.	
AB	$PEO_{0.79k}$-*b*-$PBO_{0.65k}$	0.55	n.d.	70	3.5×10^{-2}	n.d.	82
ABA	$PEO_{0.57k}$-*b*-$PBO_{0.72k}$-*b*-$PEO_{0.57k}$	0.61	n.d.	13	3.8×10^{-1}	n.d.	
AB	$PEO_{4.5k}$-*b*-$PPO_{2.1k}$	0.68	n.d.	48	n.d.	n.d.	83
ABA	$PEO_{2.3k}$-*b*-$PBO_{2.0k}$-*b*-$PEO_{2.3k}$	0.7	n.d.	4.2	n.d.	n.d.	
AB	$PEO_{1.8k}$-*b*-$PBO_{0.58k}$	0.76	n.d.	n.d.	7.0×10^{-1}	n.d.	84
ABA	$PEO_{0.92k}$-*b*-$PBO_{0.58k}$-*b*-$PEO_{0.92k}$	0.76	n.d.	n.d.	7	n.d.	
BAB	$PBO_{0.29k}$-*b*-$PEO_{1.8k}$-*b*-$PBO_{0.29k}$	0.76	n.d.	n.d.	6.8×10^{1}	n.d.	
AB	$PEO_{1.1k}$-*b*-$PPO_{1.7k}$	0.4	n.d.	n.d.	1	n.d.	
ABA	$PEO_{0.57k}$-*b*-$PPO_{1.7k}$-*b*-$PEO_{0.57k}$	0.4	n.d.	n.d.	1.5×10^{1}	n.d.	
BAB	$PPO_{0.81k}$-*b*-$PEO_{1.1k}$-*b*-$PPO_{0.81k}$	0.39	n.d.	n.d.	3.9×10^{2}	n.d.	
AB	$PEO_{4.0k}$-*b*-$PBO_{0.72k}$	0.85	n.d.	31	n.d.	n.d.	
BAB	$PBO_{0.36k}$-*b*-$PEO_{4.0k}$-*b*-$PBO_{0.36k}$	0.85	n.d.	14	n.d.	n.d.	
AB	$PEO_{1.8k}$-*b*-$PBO_{0.72k}$	0.71	n.d.	49	n.d.	n.d.	
BAB	$PBO_{0.36k}$-*b*-$PEO_{1.7k}$-*b*-$PBO_{0.36k}$	0.7	n.d.	19	n.d.	n.d.	
ABA	$PEO_{0.57k}$-*b*-$PPO_{1.7k}$-*b*-$PEO_{0.57k}$	0.4	n.d.	88	9.0×10^{-1}	n.d.	85
BAB	$PPO_{0.81k}$-*b*-$PEO_{1.1k}$-*b*-$PPO_{0.81k}$	0.39	n.d.	10	9.1×10^{1}	n.d.	
ABA	$PEG_{1.1k}$-*b*-$PCL_{2.0k}$-*b*-$PEG_{1.1k}$	0.52	34.6	n.d.	2.0×10^{-3}	n.d.	86
BAB	$PCL_{1.0k}$-*b*-$PEG_{2.0k}$-*b*-$PCL_{1.0k}$	0.5	22.2	n.d.	3.9×10^{-3}	n.d.	
ABA	$PEG_{1.1k}$-*b*-$PCL_{4.0k}$-*b*-$PEG_{1.1k}$	0.35	35.6	n.d.	1.6×10^{-3}	n.d.	
BAB	$PCL_{2.0k}$-*b*-$PEG_{2.0k}$-*b*-$PCL_{2.0k}$	0.33	35.3	n.d.	3.3×10^{-3}	n.d.	
ABA	$PEG_{2.0k}$-*b*-$PCL_{8.0k}$-*b*-$PEG_{2.0k}$	0.33	47.7	n.d.	1.4×10^{-3}	n.d.	
BAB	$PCL_{4.0k}$-*b*-$PEG_{4.0k}$-*b*-$PCL_{4.0k}$	0.33	59.5	n.d.	2.0×10^{-3}	n.d.	
ABA	$PNIPAAm_{36k}$-*b*-$PHEMA_{9.6k}$-*b*-$PNIPAAm_{36k}$	0.88	180	n.d.	4.1×10^{-2}	spherical micelles	87
BAB	$PHEMA_{4.8k}$-*b*-$PNIPAAm_{72k}$-*b*-$PHEMA_{4.8k}$	0.88	140	n.d.	5.0×10^{-2}	flower micelles	
AB	$mPEG_{2.0k}$-*b*-$PNIPAm_{16k}$	0.11	70	n.d.	n.d.	n.d.	93
BAB	$PNIPAm_{16k}$-*b*-$PEG_{4.0k}$-*b*-$PNIPAm_{16k}$	0.11	54	n.d.	n.d.	flower micelles	

[a] molecular weight composition of hydrophilic groups derived from the M_n (molecular weight) as determined by NMR. [b] hydrodynamic diameter obtained from DLS measurements. [c] aggregation number. [d] critical micelle concentration. [e] not determined.

This section first describes the differences in the CMCs of amphiphilic AB, ABA, and BAB copolymers. CMC is defined as the concentration at which almost all amphiphilic molecules in a solution form micelles. A similar concept to CMC is critical aggregation concentration (CAC). Originally, CAC referred to the concentration of a surfactant that could complex with polymers. While CMC and CAC are often confused, in this context we focus on CMC to elucidate the self-assembly behavior of the polymers themselves. The relationships between AB, ABA, and BAB polymers and their CMCs have been comprehensively summarized by Booth's research group.[81, 82, 83, 84] They studied the CMC of AB, ABA, and BAB polymers where the hydrophilic group (A) consisted of poly(ethylene oxide) (PEO), and the hydrophobic group (B) consisted of various poly(alkylene oxide) chains such as polypropylene oxide, 1,2-butylene oxide, or styrene oxide. Consequently, regardless of the type of hydrophobic component, the CMC values consistently showed the following trend AB << ABA < BAB. Two key observations can be made regarding the relationships between AB, ABA, and BAB polymers and their CMCs in aqueous

solutions. First, compared with diblock polymers, ABA and BAB polymers have higher CMC values and an entropic disadvantage related to their conformation. Specifically, triblock polymers have two hydrophilic-hydrophobic chain junctions at the core/fringe interface of the micelle, whereas diblock polymers have one. Thus, triblock polymers experience more restrictions on polymer chain movement, resulting in an unfavorable entropy, leading to an increased CMC. Second, BAB polymers have higher CMC values than ABA polymers because of the hydrophobic segments at both ends of the polymer chains, resulting in entropy loss during micellization.[85, 86] Kim and coworkers also performed simulations comparing the micellization behaviors of ABA and BAB polymers,[87] verifying that the entropy loss from the loop structure of the intermediate block in BAB polymers hindered their self-assembly ability, resulting in a higher CMC. Additionally, triblock polymers inherently have more junction points at the micelle core/fringe interface than diblock polymers, resulting in increased unfavorable entropy for the polymer chains. These findings underscore the key role of the arrangement of hydrophilic and hydrophobic moieties in modulating the CMC, highlighting the major influence of the order of polymer blocks on the entropy and overall behavior of the polymers.

Differences in the N_{agg} of polymers obtained from the self-assembly of amphiphilic AB, ABA, and BAB polymers are discussed in this section. Booth and colleagues have investigated the relationships between N_{agg} and these polymers and found multiple associations.[81, 82, 83, 84] Overall, they observed a general relationship among the polymers: BAB < ABA < AB. This order indicates that triblock polymers have a lower N_{agg} relative to diblock polymers. Furthermore, BAB polymers with hydrophobic moieties at both ends of the polymer chains exhibit lower N_{agg} values compared with ABA polymers, which are terminated by hydrophilic moieties. Therefore, an opposite trend is observed between N_{agg} and CMC, suggesting that the underlying influence is polymer chain entropy, as previously mentioned regarding the CMC. BAB polymers, which are characterized by unfavorable polymer chain entropy, exhibit high CMC values, indicating a low tendency to form micelles from the monomeric state. This means that polymer chain aggregation is suppressed, implying that N_{agg} is minimal in BAB polymers.

Next, we compare the hydrodynamic diameters (D_h) of ABA and BAB triblock polymer assemblies. Zhao *et al.* prepared ABA and BAB triblock polymers consisting of *N*-isopropylacrylamide as the hydrophilic block (A) and 2-hydroxyethyl methacrylate as the hydrophobic block (B) and found that the D_h was 140 nm for BAB polymer micelles and 180 nm for ABA polymer micelles.[88] Similarly, Liu *et al.* examined the sizes of micelles obtained from ABA and BAB polymers, using poly[*N*, *N*-(dimethylamino)ethyl methacrylate] (PDMAEMA) and poly[2-(2-methoxyethoxy)ethyl methacrylate] as the hydrophilic (A) and hydrophobic (B) segments, respectively.[89] Although similar molecular weights were maintained in their hydrophilic and hydrophobic domains, the BAB polymers manifested smaller micelles (D_h of 70 nm) compared with the ABA polymers (D_h up to 250 nm). This is attributed to the unique architecture of the BAB polymers, with hydrophobic segments capping both ends of the central hydrophilic segment. Such polymers self-assemble into relatively small micelles with flower configurations, unlike ABA polymers.[90] Flower micelles are one of the nanostructures formed by the self-assembly of BAB polymers, as evidenced by a change in micellar morphology characterized by internally looped hydrophilic segments and a compact hydrophobic core, resulting in smaller micelles relative to the swollen, expanding corona exhibited by ABA polymers.[91, 92, 93, 94] Notably, BAB polymers undergo a transformation from flower micelles to hydrogels with increasing polymer concentration, demonstrating a tendency toward higher-order structures due to intrinsic polymer chain dynamics and interactions with solvents.[95, 96] This structural change involves the increasing density of loop structures and the subsequent intrusion of hydrophobic segments into the core, promoting gelation (**Fig. 2**).

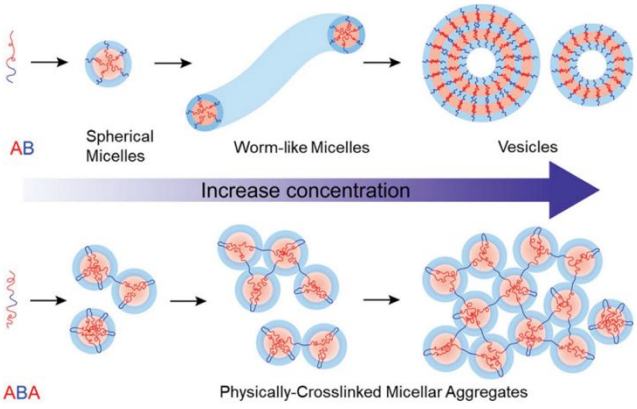

Fig. 2 Schematic illustration of different self-assembly behaviors for structures composed of AB diblock and ABA triblock copolymers at different polymer concentrations. Reproduced with permission.[96] Copyright 2020, Royal Society of Chemistry.

In this section, we compared the CMCs, N_{agg} values, sizes, and morphologies of amphiphilic linear AB, ABA, and BAB polymers. The simple addition of hydrophilic or hydrophobic blocks to AB polymers changes the entropy of the polymer chains, affecting the CMC and N_{agg} values. In addition, when hydrophilic groups were present at both ends of the polymer chain, as opposed to hydrophobic groups, variations in the size and morphology of self-assembled structures occurred. From these results, simply adding a hydrophilic or hydrophobic block to AB polymers results in significantly different self-assembly behaviors. Furthermore, these changes in self-assembly behavior were attributed to changes in polymer chain entropy caused by the modification of the polymer structure and variations in the conformation of the polymer chains within the self-assembled structures.

3-2. Comparison of self-assembly behavior between linear block copolymers and cyclic copolymers in aqueous solutions

Here, we compare the self-assembly behavior of amphiphilic cyclic polymers, in addition to that of the

amphiphilic diblock polymers and triblock polymers described above. We clarify the influence of specific polymer structures, such as the presence or absence of polymer chain ends and cyclic structures, on the self-assembly behavior (**Table 2**).

A detailed study comparing the self-assembly behavior of linear and cyclic polymers in aqueous solutions was performed by Booth and colleagues.[97, 98] They synthesized three types of polymers: a cyclic diblock polymer (cyclic-$PEO_{1.8k}$-*b*-$PBO_{0.6k}$), a linear diblock polymer ($PEO_{1.8k}$-*b*-$PBO_{0.6k}$), and a triblock polymer ($PEO_{0.9k}$-*b*-$PBO_{0.6k}$-*b*-$PEO_{0.9k}$). The CMCs, N_{agg} values, and hydrodynamic radii (R_h) were compared, revealing that micelles formed by cyclic polymers exhibited higher N_{agg} and R_h values compared with those formed by linear triblock polymers. However, these values were lower than those observed in micelles derived from linear diblock polymers. In terms of CMC, cyclic polymers and linear triblock polymers showed similar values, which were approximately 10 times higher than those of linear diblock polymers (cyclic-$PEO_{1.8k}$-*b*-$PBO_{0.6k}$: CMC = 3.0 mg mL^{-1}, R_h = 4.4 nm, N_{agg} = 16; $PEO_{0.9k}$-*b*-$PBO_{0.6k}$-*b*-$PEO_{0.9k}$: CMC = 3.0 mg mL^{-1}, R_h = 4.0 nm, N_{agg} = 6; $PEO_{1.8k}$-*b*-$PBO_{0.6k}$: CMC = 3.0 × 10^{-1} mg mL^{-1}, R_h = 10 nm, N_{agg} = 90). These findings demonstrate the variation in micelle properties, despite the polymers having similar molecular weights and hydrophilic-to-hydrophobic ratios. The authors attribute these differences to the conformational variations of the polymer chains within the micelles. They explain that linear diblock polymers possess a single core-fringe interface per polymer chain within the micelle. In contrast, linear triblock polymers and cyclic polymers feature two such interfaces per polymer chain, resulting in more restricted movement of their polymer chains, rendering the assembly entropically less favorable. Therefore, linear diblock polymers have a greater propensity to form micelles, because it is more entropically favorable owing to their structural simplicity. This is supported by their lower CMCs and N_{agg} values compared with those of their linear triblock and cyclic counterparts.[99]

The conformation of the polymer chain significantly influences micelle size. For linear triblock and cyclic polymers, a loop conformation of the polymer chain is adopted during micelle formation. This conformational change effectively shortens the chain length, leading to the formation of micelles with smaller hydrodynamic diameters. In contrast, linear diblock polymers are not subject to such conformational constraints, allowing them to have a more elongated chain morphology. As a result, micelles formed from linear diblock polymers exhibit a larger particle size compared with those formed from triblock and cyclic polymers. The self-assembly behaviors of amphiphilic cyclic polymers and linear polymers have been compared,[100] revealing that micelles formed from cyclic polymers had smaller sizes compared with those formed from linear polymers (*c*-$PEG_{2.1k}$-*b*-$PCL_{3.3k}$: D_h = 15 nm, *l*-$PEG_{2.1k}$-*b*-$PCL_{3.3k}$: D_h = 27 nm). Furthermore, Yamamoto *et al.* compared linear triblock copolymers composed of PEO and either poly(*n*-butyl acrylate) (PBA) or poly(methyl acrylate) (PMA) with cyclic diblock copolymers. Their findings showed that micelles formed from linear triblock copolymers have larger D_h and N_{agg} values compared with those formed from cyclic diblock copolymers.[101] This difference is attributed to reduced repulsive interactions between micelles, likely due to intermicellar bridging.

Some reports have considered the differences between micelle structures. Kyuyoung and colleagues synthesized amphiphilic cyclic poly(*n*-butyl acrylate-*b*-ethylene oxide) (cyclic $PBA_{1.5k}$-*b*-$PEO_{3.1k}$) and amphiphilic linear poly(*n*-butyl acrylate-*b*-ethylene oxide) (linear $PBA_{0.74k}$-*b*-$PEO_{3.1k}$-*b*-$PBA_{0.74k}$) polymers, and for the first time, the micellar structures of these polymers were analyzed in aqueous solution by synchrotron X-ray scattering (**Fig. 3**).[102] They elucidated not only the micelle size and aggregation number but also the internal structures, such as core and shell radii, and core and shell densities. As a result, linear $PBA_{0.74k}$-*b*-$PEO_{3.1k}$-*b*-$PBA_{0.74k}$ exhibited a diameter of 13.0 nm, an aggregation number of 11.61, core radii ranging from 1.85 to 1.94 nm, shell radii ranging from 4.62 to 4.65 nm, core densities ranging from 0.93 to 1.08 g cm^{-3}, and a shell density of 0.05 g cm^{-3}. Conversely, cyclic $PBA_{1.5k}$-*b*-$PEO_{3.1k}$ had a diameter of 12.5 nm, an aggregation number of 10.02, core radii ranging from 1.69 to 1.78 nm, shell radii ranging from 4.13 to 4.27 nm, core densities ranging from 1.06 to 1.23 g cm^{-3}, and a shell density of 0.06 g cm^{-3}. These results indicate that the micelles formed by cyclic polymers are not only smaller in size and aggregation number but also have a more densely packed core and shell structure compared with those formed by linear polymers. The authors suggested that the difference in polymer topology plays a critical role in the formation of high-density micelles. Specifically, because they lack terminal ends, cyclic polymers bring about lower entropy and excluded volume effects compared with their linear counterparts, allowing for more favorable hydrophobic interactions within and between polymer chains, thus maintaining the orderly packing of polymer chains and promoting denser micelles.

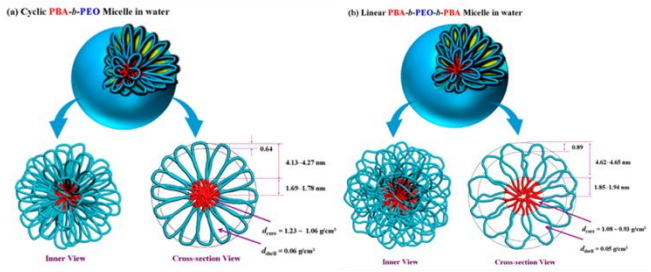

Fig. 3 Schematic illustration of structural parameters for micelles composed of (a) cyclic $PBA_{1.5k}$-*b*-$PEO_{3.1k}$ and (b) linear $PBA_{0.74k}$-*b*-$PEO_{3.1k}$-*b*-$PBA_{0.74k}$ polymers revealed by synchrotron X-ray scattering. Reproduced with permission.[102] Copyright 2014, American Chemical Society.

Several studies have compared the micelle properties of cyclic and linear polymers by performing X-ray scattering.[103, 104, 105, 106] These studies have consistently shown that simple cyclization of linear polymers leads to changes in the morphology of self-assembled structures on the nanometer to micrometer scales. Such differences are attributed to the limited packing of polymer chains in cyclic polymers, which makes their packing entropically unfavorable compared with that of linear polymers that have freely moving terminal

Table 2. The self-assembly behaviors of linear and cyclic polymers.

macromolecular architecture	polymer	$f_{hydrophilic}$	hydrodynamic diameter (nm)	N_{agg}	CMC (mg/mL)	morphology	Reference(s)
AB	$PEO_{1.8k}$-*b*-$PBO_{0.6k}$	0.76	20	90	3.0×10^{-1}	n.d.	
ABA	$PEO_{0.9k}$-*b*-$PBO_{0.6k}$-*b*-$PEO_{0.9k}$	0.76	8	6	3	n.d.	97, 98
cyclic	cyclic-$PEO_{1.8k}$-*b*-$PBO_{0.6k}$	0.76	8.8	16	3	n.d.	
AB	$PS_{9.4k}$-*b*-$PMPCS_{21k}$	0.31	33.8	100	7.3×10^{-3}	spherical micelles	99
cyclic	*c*-$PS_{9.4k}$-*b*-$PMPCS_{21k}$	0.31	38	58	1.5×10^{-2}	spherical micelles	
AB	*l*-$PEG_{2.1k}$-*b*-$PCL_{3.3k}$	0.39	27	n.d.	n.d.	n.d.	100
cyclic	*c*-$PEG_{2.1k}$-*b*-$PCL_{3.3k}$	0.39	15	n.d.	n.d.	n.d.	
BAB	$PMA_{1.4k}$-*b*-$PEO_{3.2k}$-*b*-$PMA_{1.4k}$	0.53	19	73	8.0×10^{-2}	n.d.	101
cyclic	$PMA_{2.6k}$-*b*-$PEO_{3.0k}$	0.54	14	63	9.0×10^{-2}	n.d.	
BAB	$PBA_{0.74k}$-*b*-$PEO_{3.1k}$-*b*-$PBA_{0.74k}$	0.68	13	11.6	n.d.	n.d.	102
cyclic	$PBA_{1.5k}$-*b*-$PEO_{3.1k}$	0.67	12.5	10	n.d.	n.d.	
AB	*l*-$PEO_{5.5k}$-*b*-$PBA_{1.2k}$	0.82	17	24.3	n.d.	prolate-ellipsoidal micelles	106
BAB	*l*-$PBA_{0.6k}$-*b*-$PEO_{3.0k}$-*b*-$PBA_{0.6k}$	0.67	12.5	9.1	n.d.	oblate-ellipsoidal micelles	
cyclic	*c*-$PBA_{1.3k}$-*b*-$PEO_{3.0k}$	0.67	12.1	8.9	n.d.	oblate-ellipsoidal micelles	
linear graft (linear-*g*-linear)	polycarbonate-*g*-$PNAM_{50}$	0.95	7.7	<1	n.d.	unimolecular spherical micelles	107
cyclic graft (cyclic-*g*-linear)	*c*-polycarbonate-*g*-$PNAM_{50}$	0.95	10	<1	n.d.	cylindrical unimolecular micelles	
linear	linear-$(PS_{0.8k}$-*b*-$PAA_{1.9k})_2$	0.7	22	147	n.d.	n.d.	109
8-shaped	cyclic-$(PS_{0.8k}$-*b*-$PAA_{1.9k})_2$	0.7	28	122	n.d.	n.d.	
linear	linear-$(PS_{1.5k}$-*b*-$PAA_{2.0k})_2$	0.57	70	367	n.d.	n.d.	
8-shaped	cyclic-$(PS_{1.5k}$-*b*-$PAA_{2.0k})_2$	0.57	92	250	n.d.	n.d.	
AB	$POEGMA_{5.0k}$-*b*-$PCL_{3.0k}$	0.63	55.8	n.d.	1.7×10^{-2}	spherical micelles	111, 113
Tadpol (cyclic-*b*-linear)	*c*$POEGMA_{5.0k}$-*b*-$PCL_{2.7k}$	0.65	29.5	n.d.	6.2×10^{-3}	spherical micelles	
Figure-8 (cyclic-*b*-cyclic)	*c*$POEGMA_{5.0k}$-*b*-*c*$PCL_{2.6k}$	0.66	117	n.d.	5.7×10^{-3}	spherical micelles	
AB	$mPEG_{2.0k}$-*b*-$PCL_{1.1k}$	0.63	134	n.d.	1.6×10^{-2}	spherical micelles	112
tadpole (linear-*b*-cyclic)	$mPEG_{2.0k}$-*b*-*c*$PCL_{1.1k}$	0.63	147	n.d.	9.0×10^{-3}	spherical micelles	
AB	$PEG_{2.0k}$-*b*-$PCL_{2.6k}$	0.43	155	n.d.	8.0×10^{-3}	n.d.	114
dumbbell (cyclic-*b*-linear-*b*-cyclic)	*c*$PCL_{2.6k}$-*b*-$PEG_{2.0k}$-*b*-*c*$PCL_{2.6k}$	0.27	159	n.d.	2.0×10^{-3}	n.d.	

ends. Consequently, cyclic polymers exhibit a range of morphologies from spherical to worm-like micelles and vesicles at different polymer concentrations, highlighting the unique structural versatility of cyclic polymers in nano and microscale self-assembly.

More recently, comparisons have been made not only between the self-assembly behavior of simple linear and cyclic polymers but also between more complex linear and cyclic graft polymers. O'Reilly *et al.* synthesized linear and cyclic graft polymers with a hydrophobic polycarbonate backbone

and a hydrophilic poly(*N*-acryloylmorpholine) (PNAM) side chain and compared their self-assembly behaviors in aqueous solutions (**Fig. 4**).[107] The results showed that both types of grafted polymers formed unimolecular micelles in aqueous solutions, regardless of the degree of polymerization of the PNAM chain, which was 30, 50, or 110. A combination of small-angle X-ray scattering (SAXS) and dynamic light scattering (DLS) revealed that all linear graft polymers formed spherical unimolecular micelles, whereas cyclic graft polymers formed cylindrical unimolecular micelles with side-chain polymerization degrees of 50 and 110. Thus, differences in the self-assembly behaviors of linear and cyclic graft polymers led to significant variations in the resulting morphologies. However, it was not clarified why cylindrical unimolecular micelles were formed by cyclic graft polymers only when the degree of side-chain polymerization was changed. Therefore, further studies are necessary.

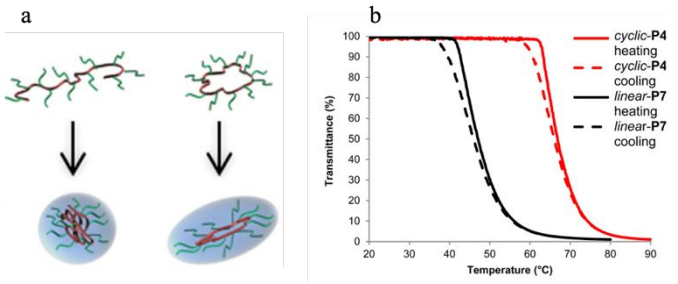

Fig. 4 (a) Schematic of the different morphologies for micelles obtained from linear and cyclic graft polymers. (b) Changes in thermal response behavior of cyclic and linear graft structures. Reproduced with permission.[107] Copyright 2016, American Chemical Society.

Recent advances in synthetic technology have made it possible to synthesize not only simple amphiphilic cyclic block polymers but also more complex polymers with cyclic structures. These include bicyclic,[108, 109] tricyclic, and tetracyclic block polymers,[110] as well as tadpole polymers,[111, 112, 113, 114, 115, 116] which are combinations of cyclic and linear polymers, and cyclic comb polymers.[117] Beyond synthesis, studies have also explored how these intricate topological differences affect self-assembly behavior. For example, Kang *et al.* synthesized various cyclic copolymers, such as amphiphilic tadpole-shaped polymers (PEG-*b*-*c*PCL), amphiphilic dumbbell-shaped polymers (*c*PCL-*b*-PEG-*b*-*c*PCL), and amphiphilic linear block polymers (PEG-*b*-PCL), and then compared their CMCs and D_h values in aqueous solutions.[112, 114] They found that an increase in the number of ring structures resulted in a decrease in the CMC and an increase in the D_h. A plausible explanation for the decrease in CMC is that the additional steric hindrance requires fewer polymer chains to reach equilibrium during micelle formation. For D_h, it was observed that cyclic structures in the hydrophilic group increased the steric hindrance and the area occupied by each polymer chain in the hydrophilic region, resulting in a larger micelle size. In several polymers, such as the figure-8 structure with two cyclic components, the effect of steric hindrance becomes more pronounced. This interference affects the packing of polymer chains, potentially leading to an increase in polymer size.[109] In comparison, tadpole polymers consistently exhibited lower CMCs than linear polymers, and the D_h values showed different trends depending on whether the cyclic structure was hydrophilic or hydrophobic, indicating that the nature of the cyclic moiety (hydrophilic or hydrophobic) significantly influences the self-assembly behavior of amphiphilic tadpole polymers.[111, 112, 113, 114] Not only have simple amphiphilic tadpole copolymers been developed, but also those that are responsive to external stimuli. These advanced tadpole copolymers, featuring disulfides at the junction points between cyclic PEG and linear polystyrene, can self-assemble into vesicular structures.[116] These assemblies collapse upon the addition of reducing agents. Such responsive copolymers hold great potential for a variety of applications, including serving as drug delivery carriers.

Although it is not directly correlated with self-assembly behaviors in solution, linear and cyclic polymers exhibit substantial disparities in their thermal response behaviors. The following section provides a brief explanation of these differences. The literature presents conflicting trends concerning the thermal responsiveness of linear and cyclic polymers. For example, cyclic polymers tend to have lower cloud points than linear polymers.[118, 119, 120, 121] This can be attributed to the fact that linear, helical polymer chains can move freely in an aqueous solution, allowing them to form hydrogen bonds with many water molecules. However, cyclic polymers are believed to adopt a more compact configuration compared with linear polymers owing to the restricted polymer chain conformation. Consequently, cyclic polymers have fewer hydrogen bonds with water molecules, resulting in a lower cloud point compared with linear polymers. Conversely, other studies have reported that cyclic polymers tend to have a higher cloud point than linear polymers.[122, 123, 124, 125] There are two possible reasons. First, this is attributed to hindered intermolecular connectivity at the topological level, resulting in repulsive forces between cyclic polymers. Second, topological constraints associated with the cyclic structure can influence dehydration and induce the collapse from coil to globule conformations upon heating.

Regarding the thermal response of amphiphilic cyclic polymers and amphiphilic linear polymers, cyclic polymers exhibit significantly higher cloud points and thermal stability compared with linear polymers. Tezuka *et al.* synthesized amphiphilic triblock polymers consisting of PEO as the hydrophilic segment and PBA as the hydrophobic segment (*l*-PBA-*b*-PEO-*b*-PBA), as well as amphiphilic cyclic polymers (*c*-PBA-*b*-PEO).[92, 101] Subsequently, a comparison of thermal stability in aqueous solution showed that micelles composed of cyclic polymers have a higher cloud point above 40 °C and improved thermal stability, even though the molecular weight composition ratio of hydrophilic and hydrophobic groups in both polymers is comparable. This may be due to the different conformations of the polymer chains forming the micelles. The

amphiphilic triblock polymers have hydrophobic groups (PBA) at both ends, which form the core of the micelle. Therefore, the polymer chains may fold while the hydrophobic groups at both ends come closer together to form flower micelles. However, not all polymer chains adopt the folded conformation, but one end can be released from one micelle core and enter another micelle core, bridging the micelles. As a result, when dehydration and summation are accelerated by increasing the temperature, aggregates form between the micelles, indicating a cloud point. In contrast, cyclic polymers cannot adopt such a conformation with bridges between micelles. Therefore, cyclic polymers require higher temperatures than linear triblock polymers to form micellar aggregates that exhibit a cloud point. As a result, they found that the micelles formed by amphiphilic cyclic polymers had higher thermal stability than those formed by amphiphilic triblock polymers. They also found that micelles composed of amphiphilic cyclic polymers have higher salt tolerance than those composed of linear triblock polymers (**Fig. 5**).[101] Furthermore, the micelles obtained from cyclic polymers can be used as catalytic nanoreactors that can withstand high

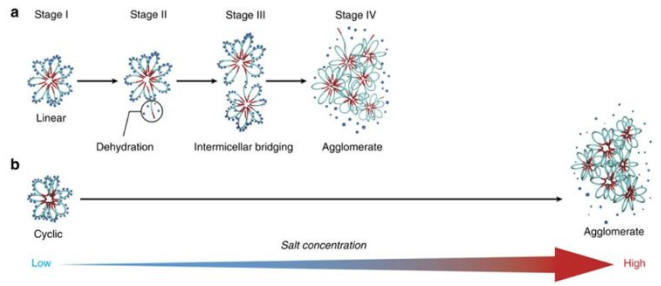

Fig. 5 Schematic representation showing how the thermal stability of a self-assembled micelle is enhanced by a topology effect. (a) *l*-PBA-*b*-PEO-*b*-PBA has hydrophobic groups at both ends, resulting in a lower cloud point owing to intermicellar cross-linking. (b) *c*-PBA-*b*-PEO has a higher cloud point because of the topological effect, having no chain ends. Reproduced with permission.[101] Copyright 2013, Nature Publishing Group.

salt concentrations. Similar to the mechanism of thermal stability described above, the salt tolerance of the cyclic polymer micelles may be due to the unique conformation of the cyclic polymers. Further studies have been conducted on the micellar mechanism of amphiphilic triblock polymers and amphiphilic cyclic polymers.[126, 127] The results showed that the enthalpy of micellization in the amphiphilic cyclic polymers was lower than that in the amphiphilic triblock polymers. This suggests that in the unimer state in aqueous solutions, the hydrophobic groups of the cyclic polymers adopt a tighter coil conformation and avoid contact with water. The entropy associated with micellization was also found to be lower for the amphiphilic cyclic polymers than for the amphiphilic triblock polymers, mainly because the triblock polymers have dangling chains (polymer chains bridging between micelles).

The linear and cyclic graft polymers mentioned above are also known to exhibit different temperature response behaviors. O'Reilly *et al*. showed that when comparing linear and cyclic grafted polymers synthesized with a degree of side-chain polymerization of 30, the linear grafted polymer had a cloud point of 47 °C, whereas the cyclic grafted polymer had a cloud point of 67 °C (**Fig. 4b**).[107] This suggests that aggregates of cyclic grafted polymers are thermodynamically more stable than aggregates of linear grafted polymers. This suggests that aggregates of cyclic grafted polymers are thermodynamically more stable than those of linear grafted polymers. This stability may be ascribed to the larger hydrodynamic volume in the cyclic grafted polymers, which allows them to interact with more water molecules. Thus, dehydration of the hydrophilic portion and aggregation of the polymer chains likely occurs at higher temperatures in cyclic graft polymers, resulting in a higher cloud point. Despite the limited number of studies, multiple cases have been reported for cyclic graft polymers with a higher cloud point than linear graft polymers.

In summary, we have reviewed the self-assembly behavior of amphiphilic cyclic polymers and amphiphilic linear polymers, from the initial research on this topic to the present, where advanced structural analysis techniques are now available. The results show that the unique topology of cyclic structures profoundly influences the internal structures, CMCs, N_{agg} values, D_h (or R_h) values, and micelle configurations. A notable difference was observed in the self-assembly behavior between amphiphilic cyclic polymers and amphiphilic linear diblock polymers. Conversely, the differences were minimal or even negligible when comparing the self-assembly behavior of amphiphilic linear triblock polymers.[98] This inconsistency may be attributed to the limited amount of research conducted in this field. Therefore, more research on the self-assembly behavior of cyclic polymers is necessary.

3-3. Comparison of self-assembly behavior between linear block copolymers and $(AB)_n$-type star block copolymers in aqueous solutions

In the previous section, we discussed the effect of the presence or absence of polymer chain ends on the self-assembly behavior by comparing linear and cyclic polymers. Here, we compare the self-assembly behavior between amphiphilic linear polymers and amphiphilic star block copolymers ($(AB)_n$-type star polymers). These $(AB)_n$-type star polymers consist of multiple AB diblock polymers linked together at a branching point. Therefore, we investigate how the self-assembly behavior is affected as the number of AB diblock polymers within the polymer chains increases (**Table 3**).

Considering the self-assembly behaviors of amphiphilic linear polymers and amphiphilic star polymers, a significant difference is observed in the CMC. For instance, Kim *et al.* developed amphiphilic diblock copolymers ($PEG_{5.0k}$-*b*-$PCL_{4.8k}$) using poly(ethylene glycol) (PEG) as the hydrophilic group and poly(ε-caprolactone) (PCL) as the hydrophobic group. They synthesized 3-arm star copolymers (($PEG_{5.0k}$-*b*-$PCL_{4.8k}$)$_3$) and 4-arm star copolymers (($PEG_{4.9k}$-*b*-$PCL_{5.1k}$)$_4$), comparing the effect of different arm numbers on the CMC.[128] The results showed that the CMC of the $PEG_{5.0k}$-*b*-$PCL_{4.8k}$ linear polymer was 2.15 × 10^{-3} mg mL^{-1}, that of the 3-arm star ($PEG_{5.0k}$-*b*-$PCL_{4.8k}$)$_3$ was 1.43 × 10^{-3} mg mL^{-1}, and that of the 4-arm star ($PEG_{4.9k}$-*b*-$PCL_{5.1k}$)$_4$

was 7.54 × 10^{-4} mg mL^{-1}. Moreover, Lim *et al.* synthesized 4- and 6-arm star copolymers, (($PEG_{4.7k}$-*b*-$PCL_{5.5k}$)$_4$) and (($PEG_{4.6k}$-*b*-$PCL_{5.3k}$)$_6$), respectively, and examined their CMCs.[129] They found that the 4-arm star ($PEG_{4.7k}$-*b*-$PCL_{5.5k}$)$_4$ had a CMC of 7.57 × 10^{-4} mg mL^{-1}, and the 6-arm star ($PEG_{4.6k}$-*b*-$PCL_{5.3k}$)$_6$ had a CMC of 4.25 × 10^{-4} mg mL^{-1}. This trend of decreasing CMC with an increasing number of arms is not restricted to block copolymers combining PEG and PCL. Liu *et al.* synthesized amphiphilic polymers with 1, 2, 4, and 6 arms, consisting of poly(L-lactide) (PLLA) I as the hydrophobic group and PEO as the hydrophilic group, comparing their CMCs in aqueous solutions.[130] The CMC was found to decrease as the number of arms increased, a trend reported by various researchers.[131, 132, 133, 134] In contrast, Hyun *et al.* synthesized polymers with 1, 2, 4, and 8 arms composed of PEG and PCL and found that the CMC increased with the increasing number of arms.[135] This contradiction may originate from the positioning of hydrophilic and hydrophobic groups. Specifically, in polymers where the hydrophobic groups are internal and the hydrophilic groups are external, an increase in arms leads to a decrease in entropy during micellization. Conversely, in polymers where the hydrophobic groups are external, the polymers have to fold to prevent the hydrophobic groups from interacting with the solvent (water), resulting in an increased entropy and a higher CMC. Thus, the structural arrangement of the hydrophilic and hydrophobic groups influences the CMC of star polymers.

Differences in the self-assembly behavior of linear and star polymers significantly affect various physical parameters, including CMC and N_{agg}. For example, Micheal *et al.* synthesized amphiphilic diblock copolymers and 4-arm star copolymers using poly(acrylic acid)) as the hydrophilic group and poly(styrene) (PS) as the hydrophobic group and investigated their effect on N_{agg}.[136] They found that changing the polymer structure from linear to star architecture reduced the N_{agg}, with values of 303 for the linear polymer and 15 for the 4-armed star polymer, while maintaining comparable molecular weight composition ratios of the hydrophilic and hydrophobic groups. Similar trends have been observed for other polymer combinations. Alhoranta *et al.* synthesized amphiphilic triblock copolymers and 6-arm star polymers consisting of PDMAEMA as the hydrophilic group and either PS or PBA as the hydrophobic group, and then compared their self-assembly behavior.[137] The $PDMAEMA_{31k}$-*b*-PS_{31k}-*b*-$PDMAEMA_{31k}$ and $PDMAEMA_{31k}$-*b*-PBA_{31k}-*b*-$PDMAEMA_{31k}$ linear triblock polymers exhibited N_{agg} values of 265 and 88, respectively, whereas the ($PDMAEMA_{13k}$-*b*-$PS_{4.2k}$)$_6$ and ($PDMAEMA_{13k}$-*b*-$PBA_{4.2k}$)$_6$ 6-arm star copolymers exhibited N_{agg} values of 22 and 34, respectively. Furthermore, Tirelli *et al.* synthesized amphiphilic diblock, triblock, and star polymers with 4, 6, and 8 arms, using PEG as the hydrophilic group and poly(propylene sulfide) as the hydrophobic group, and compared their self-assembly behaviors.[138] Consistent with previous findings, N_{agg} decreased as the number of arms increased. Taken together, these reports suggest that the N_{agg} varies with the number of arms, particularly when the molecular weight composition ratio of the hydrophilic and hydrophobic groups remains constant. This tendency may be due to folding of the polymer chains prior to micellar formation. Star diblock polymers adopt a bent conformation around a branching point prior to micellar formation. However, owing to steric repulsion between the chains, the polymer chains do not adopt a fully closed conformation, but instead adopt a slightly expanded conformation where the hydrophilic groups are exposed, increasing the surface area occupied by each polymer chain. Consequently, fewer polymer chains are required for micelle formation, resulting in a decrease in N_{agg} with an increase in the number of arms. This proposed mechanism is consistent with the observation that increasing the number of star polymer arms facilitates micelle formation, resulting in a lower CMC. In cases where increasing the number of arms tends to decrease N_{agg}, unimolecular micelles, or micelles with a N_{agg} of one, can form. Unimolecular micelles are typically derived from hyperbranched polymers, dendrimers, graft polymers, or random polymers.

The distinct self-assembly behaviors of linear and star polymers also influence the sizes of the micelles formed from each polymer. For example, Wang *et al.* synthesized linear block polymers ($PCL_{4.7k}$-*b*-$PDMAEMA_{15k}$) and 4-armed star polymers ($PCL_{1.0k}$-*b*-$PDMAEMA_{3.8k}$)$_4$ containing PCL as the hydrophobic group and PDMAEMA as the hydrophilic group and analyzed their self-assembly behavior.[139] The D_h of the micelles formed by $PCL_{4.7k}$-*b*-$PDMAEMA_{15k}$ was 210.6 nm, and that of the micelles formed by ($PCL_{1.0k}$-*b*-$PDMAEMA_{3.8k}$)$_4$ was 160.0 nm, indicating that the 4-arm star polymer micelles were smaller than those of the linear polymer. Furthermore, Stefan *et al.* synthesized linear polymers using poly(γ-benzyloxy-ε-caprolactone) as the hydrophobic group and poly(PMEECL) as the hydrophilic group, as well as 4- and 6-arm star polymers, and compared their self-assembly behaviors.[140] The D_h of the micelles obtained from the linear polymers was 108.2 nm, and that of the micelles obtained from the 4- and 6-arm star polymers was 85.30 and 52.14 nm, respectively. This shows that the micelles obtained from star polymers were significantly smaller than those from linear polymers, with the size decreasing further as the number of arms increased. This trend has been confirmed by other studies. The decrease in micelle size as the number of arms increases is potentially due to the increased tendency of the star polymers to form unimolecular micelles. As the number of arms increases, fewer polymer chains are required to form micelles, resulting in smaller micelle sizes.

Table 3. The self-assembly behaviors of linear and $(AB)_n$-type star polymers.

macromolecular architecture	polymer	$f_{hydrophilic}$	hydrodynamic diameter (nm)	N_{agg}	CMC (mg/mL)	morphology	reference
AB	$PEG_{5.0k}$-*b*-$PCL_{4.8k}$	0.51	105	n.d.	2.15×10^{-3}	n.d.	
$(AB)_3$	$(PEG_{4.9k}$-*b*-$PCL_{4.7k})_3$	0.51	115	n.d.	1.43×10^{-3}	n.d.	128
$(AB)_4$	$(PEG_{4.9k}$-*b*-$PCL_{5.1k})_4$	0.49	129	n.d.	7.54×10^{-4}	n.d.	
$(AB)_4$	$(PEG_{4.8k}$-*b*-$PCL_{2.9k})_4$	0.63	n.d.	n.d.	2.14×10^{-3}	n.d.	
$(AB)_6$	$(PEG_{7.2k}$-*b*-$PCL_{3.7k})_6$	0.64	n.d.	n.d.	1.76×10^{-3}	n.d.	129
$(AB)_4$	$(PEG_{4.7k}$-*b*-$PCL_{5.5k})_4$	0.46	n.d.	n.d.	7.57×10^{-4}	n.d.	
$(AB)_6$	$(PEG_{4.6k}$-*b*-$PCL_{5.3k})_6$	0.47	n.d.	n.d.	4.25×10^{-4}	n.d.	
AB	$PEO_{2.0k}$-*b*-$PLLA_{5.6k}$	0.27	29.4	n.d.	7.5×10^{-2}	n.d.	
ABA	$(PEO_{2.0k}$-*b*-$PLLA_{4.4k})_2$	0.29	24.2	n.d.	n.d.	n.d.	130
$(AB)_4$	$(PEO_{2.0k}$-*b*-$PLLA_{4.8k})_4$	0.3	22.8	n.d.	n.d.	n.d.	
$(AB)_6$	$(PEO_{2.0k}$-*b*-$PLLA_{4.6k})_6$	0.27	21.9	n.d.	2.0×10^{-4}	n.d.	
AB	$PDEAS_{5.3k}$-*b*-$PCL_{2.3k}$	0.7	79..6	n.d.	1.1×10^{-3}	spherical micelles	
$(AB)_4$	$(PDEAS_{5.6k}$-*b*-$PCL_{2.3k})_4$	0.71	80.8	n.d.	9.65×10^{-4}	spherical micelles	131
$(AB)_6$	$(PDEAS_{5.3k}$-*b*-$PCL_{2.3k})_6$	0.7	63.6	n.d.	8.61×10^{-4}	spherical micelles	
AB	$PCL_{7.2k}$-*b*-$PMEEECL_{1.8k}$	0.2	96.4	n.d.	1.20×10^{-3}	spherical micelles	132
$(AB)_4$	$(PCL_{7.2k}$-*b*-$PMEEECL_{1.8k})_4$	0.28	66.9	n.d.	5.62×10^{-4}	spherical micelles	
$(AB)_3$	$(PEG_{4.0k}$-*b*-$PLGA_{4.2k})_3$	0.49	n.d.	n.d.	6.30×10^{-3}	spherical micelles	
$(AB)_4$	$(PEG_{4.0k}$-*b*-$PLGA_{4.6k})_4$	47	n.d.	n.d.	3.16×10^{-3}	spherical micelles	133
$(AB)_6$	$(PEG_{4.0k}$-*b*-$PLGA_{4.3k})_6$	0.48	n.d.	n.d.	1.78×10^{-3}	spherical micelles	
AB	$PEG_{2.0k}$-*b*-$PCL_{2.1k}$	0.49	n.d.	n.d.	1.26×10^{-3}	n.d.	
BAB	$PCL_{1.1k}$-*b*-$PEG_{2.0k}$-*b*-$PCL_{1.1k}$	0.48	n.d.	n.d.	2.51×10^{-3}	n.d.	135
$(AB)_4$	$(PEG_{0.50k}$-*b*-$PCL_{0.51k})_4$	0.5	n.d.	n.d.	3.98×10^{-3}	n.d.	
$(AB)_8$	$(PEG_{0.25k}$-*b*-$PCL_{0.26k})_8$	0.49	n.d.	n.d.	5.62×10^{-3}	n.d.	
AB	$PS_{3.2k}$-*b*-$PAA_{9.5k}$	0.75	70.4	303	n.d.	spherical micelles	136
$(AB)_4$	$(PS_{3.2k}$-*b*-$PAA_{9.5k})_4$	0.75	39.1	15	n.d.	spherical micelles	
ABA	$PDMAEMA_{31k}$-*b*-PS_{31k}-*b*-$PDMAEMA_{31k}$	0.67	180	265	n.d.	spherical micelles	
ABA	$PDMAEMA_{31k}$-*b*-$PBuA_{31k}$-*b*-$PDMAEMA_{31k}$	0.67	114	88	n.d.	spherical micelles	137
$(AB)_6$	$(PDMAEMA_{13k}$-*b*-$PS_{4.2k})_6$	0.75	130	22	n.d.	spherical micelles	
$(AB)_6$	$(PDMAEMA_{13k}$-*b*-$PBuA_{4.2k})_6$	0.75	162	34	n.d.	spherical micelles	
AB	$PCL_{4.7k}$-*b*-$PDMAEMA_{15k}$	0.76	210.6	n.d.	2.12×10^{-2}	daisy flower like micelles	139
$(AB)_4$	$(PCL_{1.0k}$-*b*-$PDMAEMA_{3.8k})_4$	0.79	160	n.d.	8.01×10^{-3}	daisy flower like micelles	
AB	$PBCL_{12k}$-*b*-$PMEEECL_{12k}$	0.51	108.2	n.d.	1.23×10^{-3}	spherical micelles	
$(AB)_4$	$(PBCL_{3.0k}$-*b*-$PMEEECL_{3.0k})_4$	0.5	85.3	n.d.	2.70×10^{-4}	spherical micelles	140
$(AB)_6$	$(PBCL_{1.9k}$-*b*-$PMEEECL_{2.2k})_6$	0.54	52.14	n.d.	9.19×10^{-5}	spherical micelles	
AB	$PMA_{4.3k}$-*b*-$PGA_{7.7k}$	0.64	25	n.d.	n.d.	spherical micelles	141
$(AB)_4$	$(PMA_{7.5k}$-*b*-$PGA_{17k})_4$	0.69	210	n.d.	n.d.	vesicles	
AB	$PDMI_{4.4k}$-*b*-$PPEGMA_{2.2k}$	0.37	122	n.d.	n.d.	large compound micelles	
ABA	$PPEGMA_{0.96k}$-*b*-$PDMI_{4.4k}$-*b*-$PPEGMA_{0.96k}$	0.3	190	n.d.	n.d.	vesicles	142
$(AB)_3$	$(PDMI_{3.2k}$-*b*-$PPEGMA_{0.96k})_3$	0.34	79	n.d.	n.d.	spherical micelles	
AB	maltopentaose-*b*-$PPO_{1.5k}$	0.36	110	3.6×10^4	0.5	bilayer vesicles	143
ABA	maltopentaose-*b*-$PPO_{3.4k}$-*b*-maltopentaose	0.33	48	1.4×10^2	0.5	rod-like micelles	

3-arm	(maltopentaose-*b*-$PPO_{1.5k}$)$_3$	0.36	16	9.6	0.2	spherical micelles
cyclic graft	cycloamylose-*g*-$PPO_{1.7k}$	0.31	114	6.6× 10^3	0.1	multilamellar vesicles

Differences in the self-assembly behaviors of linear and star polymers can also influence the resulting polymer nanostructures. Whittaker *et al.* compared the self-assembly behavior of micelles derived from linear diblock polymers composed of PMA and poly(glycerol acrylate) with those derived from 4-arm star polymers.[141] The linear polymers formed spherical micelles with a D_h of 25 nm in aqueous solutions, whereas the 4-arm star polymers formed vesicles with a D_h of approximately 210 nm. However, the reasons for the morphological differences were not clearly explained. Goto and colleagues also observed that variations in polymer structures can influence morphology.[142] They synthesized linear diblock polymers ($PDMI_{4.4k}$-*b*-$PPEGMA_{2.2k}$) consisting of poly(dimethyl itaconate) (PDMI) and poly(poly(ethylene glycol) methyl ether methacrylate) (PPEGMA), as well as linear triblock polymers ($PPEGMA_{0.96k}$-*b*-$PDMI_{4.4k}$-*b*-$PPEGMA_{0.96k}$) and 3-arm star polymers (($PDMI_{3.2k}$-*b*-$PPEGMA_{0.96k}$)$_3$). The findings revealed that PDMI-b-PPEGMA formed spherical micelles with a D_h of 122 nm, whereas PDMI-b-PPEGMA-b-PDMI formed vesicles with a D_h of 190 nm, and the 3-arm PDMI-b-PPEGMA formed spherical micelles with a D_h of 79 nm. These results underscore the impact of polymer structure on the morphology of self-assembled aggregates. Furthermore, the authors identify two key reasons why only linear triblock polymers formed vesicles while both linear diblock polymers and 3-arm star polymers formed spherical micelles. First, the presence of hydrophilic groups at both ends of the linear triblock polymer facilitated the formation of single-layer vesicles. Second, the rigidity of the hydrophobic PDMI groups allowed for an efficient alignment of the polymer chains, resulting in a diminished curvature at the interface between hydrophilic and hydrophobic groups. These factors collectively enabled the linear triblock polymers to form vesicles. Recently, we synthesized various AB polymers, ABA polymers, 3-arm star polymers, and cyclic graft polymers, incorporating sugar chains as hydrophilic groups and poly(propylene oxide) (PPO) as hydrophobic groups.[143] All molecular weight composition ratios between hydrophilic and hydrophobic groups were kept consistent. AB copolymers formed bilayer vesicles, ABA copolymers formed rod-like micelles, 3-arm star copolymers formed spherical micelles, and cyclic graft copolymers formed multilamellar vesicles (**Fig. 6**). To clarify the causes behind these varied outcomes, we calculated the critical packing parameter (CPP) of the self-assemblies derived from each polymer, using data from transmission electron microscopy (TEM), SAXS, DLS, and field flow fractionation and multiangle light scattering measurements. The cross-sectional area of the interface between hydrophilic and hydrophobic groups per polymer chain (*a*) generally increased with the increasing number of arms, except for cyclic graft polymers. Owing to the excluded volume effect and the repulsion between hydrophilic groups, the polymer chains could not fully assemble and instead

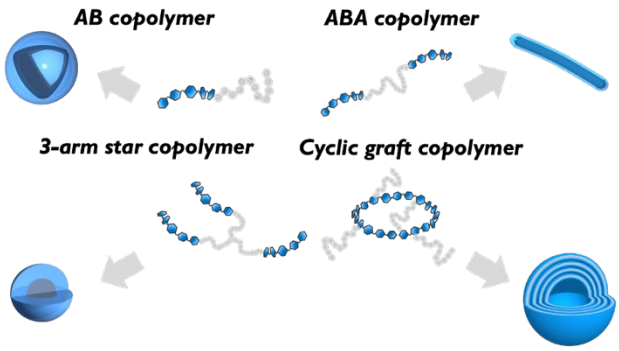

Fig. 6 Schematic illustration of the self-assembled morphologies for AB, ABA, 3-arm, and cyclic graft polymers. Reproduced with permission.[143] Copyright 2023, Royal Society of Chemistry.

assumed a slightly extended conformation. The steric hindrance, which is expected to increase as the number of arms increases, influences this behavior. Thus, the *a* value appears to increase as the number of arms increases. Additionally, the volume of the hydrophobic region occupied by each polymer chain decreased as the number of arms increased, possibly because of the fluidity of the PPO chains. In conclusion, by calculating the CPP for various polymers while maintaining the molecular weight compositions of the hydrophilic and hydrophobic groups, we elucidated how structural differences in the polymer chains determine the morphology of the self-assembled materials.

To date, we have studied variations in morphologies of self-assemblies formed by pre-synthesized linear and star polymers when dispersed in aqueous solutions. However, a contrasting approach, polymerization-induced self-assembly (PISA), has also been investigated to discern the influence of differences in polymer structure on the morphology of self-assemblies. In PISA, amphiphilic polymers are synthesized *in situ* in aqueous solutions, resulting in self-assemblies that are predominantly driven by kinetics and may not strictly follow the rules outlined above. For example, Stoffelbach *et al.* investigated how different structures of polymeric RAFT agents affect PISA under aqueous dispersion conditions.[144] Amphiphilic AB diblock, $(AB)_2$ triblock, and three-armed star $(AB)_3$ copolymers consisting of *N,N*-dimethylacrylamide (A block), and diacetone acrylamide (B block) were synthesized, and the morphologies of the assemblies were compared. A wide range of self-assembled morphologies formed depending on the polymer structure and length of their arms. Zhang *et al.* synthesized linear and star block polymer nano-assemblies with different numbers of arms and investigated their behavior under PISA conditions.[145] Notably, the linear polymers predominantly formed spherical micelles, whereas the 2- and 3-arm star polymers exhibited unique assemblies, such as vesicles and nanospheres, which

were not observed in the linear polymers. In contrast, the 4-arm star polymers primarily formed larger assemblies. Two significant observations were made. First, vesicles derived from 2- and 3-arm star polymers were significantly smaller than those derived from conventional linear polymers. Second, these vesicles even formed with a lower molecular weight composition ratio of hydrophobic groups, in contrast to conventional linear polymers. The formation of unique assemblies by 2- and 3-arm star polymers is attributed to increased steric repulsion, resulting in more ordered molecular assemblies. Larger assemblies observed for 4-arm star polymers are attributed to intermicellar cross-linking because of the external placement of hydrophobic groups and multiple arms. In summary, while previous discussions have predominantly focused on the influence of pre-defined polymer structures on self-assembly, PISA shows that kinetic dominance can also be a determining factor in the resulting morphology of polymer assemblies.

In the discussion above, we have compared the self-assembly behaviors of amphiphilic linear polymers and $(AB)_n$ star polymers. The two types of polymers exhibit different self-assembly behaviors, although they have similar hydrophilic-to-hydrophobic molecular weight composition ratios. In particular, several critical parameters, namely the CMC, $N_{agg,}$ and D_h, were observed to decrease with an increasing number of arms. This phenomenon can be clarified by considering both the thermodynamic and geometric perspectives. Thermodynamically, the unimer state in an aqueous solution tends to correspond with the micellar state as the number of arms increases, thus minimizing entropy loss during the micelle formation process. This transition facilitates micelle formation at lower concentrations, thereby lowering the CMC. A lower CMC also results in reduced N_{agg} and D_h values. Geometrically, an increase in the number of arms increases steric hindrances, including the excluded volume effect and repulsion between hydrophilic groups. Consequently, the ability of the hydrophilic group to surround the hydrophobic group is increased, reducing the number of polymer chains required for micelle formation. Therefore, CMC, N_{agg}, and D_h are inversely proportional to the number of arms. The increase in the number of arms also affected the CPP and changed the morphology of the self-assemblies in certain cases. Within the domain of $(AB)_n$ star polymers, variations in self-assembly behavior were also detected based on the spatial arrangement of hydrophilic and hydrophobic groups, specifically whether they were internally or externally located. In conclusion, not only the number of arms but also the organization of hydrophilic and hydrophobic groups should be carefully considered when exploiting $(AB)_n$ star polymer self-assemblies in various applications.

3-4. Comparison of self-assembly behavior between linear block copolymers and miktoarm star copolymers in aqueous solutions

In the previous section, we compared the self-assembly behavior of $(AB)_n$ star-shaped polymers with that of linear polymers. Then, we investigated how the self-assembly behavior is affected when the number of AB diblock polymers increases around the branching point. From here, we compare the self-assembly behavior of the star-shaped polymers with that of the miktoarm star-shaped polymer (A_mB_n) and linear polymers. We then consider the self-assembly behavior when the number of hydrophobic or hydrophilic arms increases around the branching point (**Table 4**).

A seminal study reported by Faust *et al.* revealed how the CMC of miktoarm polymers differs from that of the corresponding linear copolymer.[146] They synthesized a linear polymer ($PIB_{5.0k}$-*b*-$PMeVE_{20k}$) and a 4-miktoarm polymer $(PIB_{2.5k})_2$-*b*-$(PMeVE_{9.9k})_2$ composed of poly[bis(methyl vinyl ether)] (PMeVE) and poly[bis(isobutylene)] (PIB) and found that the CMC of the miktoarm star polymer was 10 times greater than its linear counterpart. The CMC tended to decrease in the miktoarm polymers compared with the findings in linear polymers. However, the reason for this observation remains unclear. Several studies have investigated how, compared with that of linear polymers, the CMC of miktoarm polymers is affected by the number of hydrophic arms. For example, Bae *et al.* synthesized and compared amphiphilic linear diblock (AB) and 3-miktoarm (AB_2) polymers using PEG as the hydrophilic group and PLLA as the hydrophobic group.[147] They revealed that the CMC of the 3-miktoarm polymers was slightly lower than that of the linear polymers, while comparable molecular weights were maintained in their hydrophilic and hydrophobic groups. This trend was consistent with the results obtained by Yoon *et al.*[148] and Yun *et al.*,[149] where branching of the hydrophobic chains resulted in a decrease in CMC. However, contrary observations have also been reported. Nie *et al.*[150] and Quaglia *et al.*[151] showed that miktoarm polymers had a higher CMC when the hydrophobic group had a branched structure. They attributed this to the entropic disadvantage at the core-corona interface due to reduced polymer chain mobility, which hinders effective micellization.

Table 4. The self-assembly behaviors of linear and miktoarm star polymers.

macromolecular architecture	polymer	$f_{hydrophilic}$	hydrodynamic diameter (nm)	N_{agg}	CMC (mg/mL)	morphology	reference(s)
AB	$PIB_{5.0k}$-*b*-$PMeVE_{20k}$	0.8	154	n.d.	6.3×10^{-1}	n.d.	146
A_2B_2	$(PIB_{2.5k})_2$-*b*-$(PMeVE_{9.9k})_2$	0.8	177	n.d.	1.1×10	n.d.	
AB	$PEG_{2.0k}$-*b*-$PLLA_{16k}$	0.11	n.d.	n.d.	6.3×10^{-4}	vesicles	147
AB_2	PEG_{2k}-*b*-$(PLLA_{8.6k})_2$	0.1	n.d.	n.d.	5.5×10^{-4}	vesicles	
AB	PEG_{2k}-*b*-$PLLA_{7.5k}$	0.21	n.d.	n.d.	1.3×10^{-3}	vesicles	
AB_2	PEG_{2k}-*b*-$(PLLA_{4.6k})_2$	0.18	n.d.	n.d.	1.1×10^{-3}	vesicles	
AB	PEG_{2k}-*b*-$PLLA_{3.3k}$	0.38	n.d.	n.d.	8.8×10^{-3}	spherical micelles, compound micelles	
AB_2	PEG_{2k}-*b*-$(PLLA_{1.8k})_2$	0.36	n.d.	n.d.	8.3×10^{-3}	vesicles	
AB	$PEG_{5.1k}$-*b*-$PLLA_{4.8k}$	0.51	n.d.	n.d.	9.1×10^{-3}	spherical micelles	
AB_2	$PEG_{5.1k}$-*b*-$(PLLA_{2.5k})_2$	0.5	n.d.	n.d.	8.9×10^{-3}	vesicles	
AB	PEG_{2k}-*b*-PCL_{10k}	0.17	84	n.d.	0.3×10^{-3}	spherical micelles	148
AB_2	PEG_{2k}-*b*-$(PCL_{4.4k})_2$	0.19	n.d.	n.d.	0.5×10^{-3}	fiber-like micelles	
AB	PEG_{2k}-*b*-$PCL_{4.7k}$	0.3	67	n.d.	1.6×10^{-3}	spherical micelles	
AB_2	PEG_{2k}-*b*-$(PCL_{2.3k})_2$	0.3	n.d.	n.d.	0.8×10^{-3}	fiber-like micelles	
AB	PEG_{2k}-*b*-$PCL_{2.1k}$	0.49	61	n.d.	2.5×10^{-3}	spherical micelles	
AB_2	PEG_{2k}-*b*-$(PCL_{0.80k})_2$	0.55	65	n.d.	1.8×10^{-3}	spherical micelles	
AB	PIB_{15k}-*b*-$PMeVE_{2.8k}$	0.16	62	900	1.0×10^{-3}	vesicle	149
AB_2	PIB_{14k}-*b*-$(PMeVE_{1.3k})_2$	0.16	110	7500	3.2×10^{-4}	vesicle	
AB	$mPEG_{1.9k}$-*b*-PSA	0.14	200	n.d.	1.0×10^{-2}	micellar aggregates	150
AB_2	$mPEG_{1.9k}$-*b*-$(PSA)_2$	0.13	300	n.d.	4.0×10^{-3}	micellar aggregates	
AB	$mPEG_{2.0k}$-*b*-$PCL_{4.3k}$	0.32	40	n.d.	3.0×10^{-4}	n.d.	151
AB_2	$mPEG_{2.0k}$-*b*-$(PCL_{2.1k})_2$	0.32	67	n.d.	6.9×10^{-4}	n.d.	
AB	$PDMA_{7.0k}$-*b*-$PCL_{6.4k}$	0.52	42	247	n.d.	spherical micelles	153
A_2B	$(PDMA_{3.4k})_2$-*b*-$PCL_{7.0k}$	0.5	22	41	n.d.	spherical micelles	
AB_2	$PDMA_{6.4k}$-*b*-$(PCL_{3.3k})_2$	0.49	34	120	n.d.	spherical micelles	
AB	PI_{48k}-*b*-PS_{47k}	0.5	91	243	n.d.	n.d.	154
AB_2	PI_{48k}-*b*-$(PS_{22k})_2$	0.52	86	130	n.d.	n.d.	
A_2B	$(PI_{21k})_2$-*b*-PS_{44k}	0.49	63	66	n.d.	n.d.	
AB	PS_{34k}-*b*-$PDMS_{15k}$	0.69	61	306	n.d.	n.d.	156
ABA	PS_{34k}-*b*-$PDMS_{30k}$-*b*-PS_{34k}	0.69	62	140	n.d.	n.d.	
A_2B	$(PS_{16k})_2$-*b*-$PDMS_{16k}$	0.67	45	191	n.d.	n.d.	
AB	$HPMC_{10k}$-*b*-PLA_{2k}	0.83	240	n.d.	n.d.	spherical micelles	157,158
A_2B	$(HPMC_{5k})_2$-*b*-PLA_{2k}	0.83	132	n.d.	n.d.	spherical micelles	
AB	MH-*b*-$PCL_{2.5k}$	0.31	34	n.d.	n.d.	spherical micelles	159
AB	MH-*b*-$PCL_{3.3k}$	0.26	44	n.d.	n.d.	spherical micelles	
AB	MH-*b*-PCL_{5k}	0.2	56	n.d.	n.d.	spherical micelles	
AB	MH-*b*-PCL_{10k}	0.11	86	n.d.	n.d.	spherical micelles	
AB_2	MH-*b*-$(PCL_{5k})_2$	0.11	98	n.d.	n.d.	large compound micelles	
AB_3	MH-*b*-$(PCL_{3.3k})_3$	0.11	112	n.d.	n.d.	large compound micelles	
A_2B_2	$(MH)_2$-*b*-$(PCL_{5k})_2$	0.18	78	n.d.	n.d.	spherical micelles	

A_2B	$(MH)_2$-*b*-PCL_{10k}	0.17	62	n.d.	n.d.	spherical micelles
A_3B	$(MH)_3$-*b*-PCL_{10k}	0.23	58	n.d.	n.d.	spherical micelles

The effect of increasing the number of hydrophilic group arms has also been examined. A study by Gnanou *et al.* found that miktoarm polymers with branched hydrophilic groups had a higher CMC, which was attributed to increased steric hindrance and energy requirements for micelle formation.[152] Overall, other inconsistent results have been reported, suggesting that the relationship between the CMC of miktoarm and linear polymers is influenced by multiple factors. Some studies suggest that increasing the number of hydrophobic arms in miktoarm polymers promotes micelle formation, whereas other studies show inhibited micelle formation. More thorough investigations are required to elucidate the underlying factors that influence the CMC in miktoarm polymers compared with that in linear polymers.

The following section discusses how the N_{agg} varies with an increase in the number of hydrophobic or hydrophilic arms. Liu *et al.* reported on an amphiphilic linear polymer ($PDMA_{7.0k}$-*b*-$PCL_{6.4k}$) using poly-2-(dimethylamino)ethyl methacrylate (PDMA) as the hydrophilic group and PCL as the hydrophobic group and synthesized two types of miktoarm polymers, namely $PDMA_{6.4k}$-*b*-$(PCL_{3.3k})_2$ and $(PDMA_{3.4k})_2$-*b*-$PCL_{7.0k}$.[153] Light scattering measurements revealed N_{agg} values of 247, 120, and 41 for $PDMA_{7.0k}$-*b*-$PCL_{6.4k}$, $PDMA_{6.4k}$-*b*-$(PCL_{3.3k})_2$, and $(PDMA_{3.4k})_2$-*b*-$PCL_{7.0k}$, respectively. It is widely recognized that N_{agg} depends on the molecular weight of the hydrophobic groups. In this study, however, the molecular weights and volume fractions of the hydrophilic and hydrophobic groups were kept identical in all polymers. Thus, the differences in N_{agg} are due to variations in the molecular architecture of the polymer chains. The decrease in N_{agg} with an increasing number of hydrophilic PDMA groups was attributed to increased steric repulsion between adjacent PDMA chains and increased curvature of the core-corona interface. As a result, each polymer chain occupied a larger surface area on the micelle, reducing the number of polymer chains needed to stabilize the micelle and resulting in a lower N_{agg}. In support of this, the surface area of the micelle occupied by each polymer chain (A_c) was determined, revealing values of 4.0, 4.8, and 7.1 for $PDMA_{7.0k}$-*b*-$PCL_{6.4k}$, $PDMA_{6.4k}$-*b*-$(PCL_{3.3k})_2$, and $(PDMA_{3.4k})_2$-*b*-$PCL_{7.0k}$, respectively. This indicates that an increase in the number of hydrophilic arms increases the micellar surface area occupied by each polymer chain, resulting in a decrease in N_{agg}. Similar trends of decreasing N_{agg} with the increasing number of hydrophilic arms have been reported for self-assembly in organic solvents.[154, 155] Aliferis *et al.* synthesized linear polymers (PS-*b*-PDMS, PS-*b*-PDMS-*b*-PS) and a 3-miktoarm polymer ($(PS)_2$-*b*-PDMS) composed of PS and poly(dimethylsiloxane) (PDMS) and investigated their self-assembly behaviors in dimethylformamide, in which PS is soluble.[156] The N_{agg} values of 306, 140, and 190 were obtained for PS-*b*-PDMS, PS-*b*-PDMS-*b*-PS, and $(PS)_2$-*b*-PDMS, respectively. Therefore, polymers with similar molecular weights but a branched structure forming the micelle shell have smaller N_{agg} values, probably because of increased steric repulsion caused by branching of the hydrophilic chains. However, uncertainties remain when comparing the self-assembly behaviors of triblock and miktoarm polymers with matched molecular weights of the hydrophilic and hydrophobic groups, necessitating further investigation.

Next, we discuss how increasing the number of hydrophilic and hydrophobic arms affects the particle size of the self-assembled structures. Deratani *et al.* showed that increasing the number of hydrophilic group arms affects the CMC, but they also revealed the impact on particle size by comparing micelles formed from amphiphilic linear polymers ($HPMC_{10k}$-*b*-PCL_{2k}) and amphiphilic multiarm polymers ($(HPMC_{5k})_2$-*b*-PCL_{2k}) consisting of hydroxyl propyl methyl cellulose (HPMC) and PCL.[157, 158] The D_h values of the micelles for $HPMC_{10k}$-*b*-PCL_{2k} and $(HPMC_{5k})_2$-*b*-PCL_{2k} were 240 and 132 nm, respectively. Similarly, in their study presented in the N_{agg} section, Liu *et al.* showed that micelles formed from miktoarm polymers with more hydrophilic group arms had smaller D_h values compared with those formed from linear polymers ($PDMA_{7.0k}$-*b*-$PCL_{6.4k}$: D_h = 42 nm, $(PDMA_{3.4k})_2$-*b*-$PCL_{7.0k}$: D_h = 22 nm).[153] In addition, Satoh *et al.* synthesized various amphiphilic miktoarm polymers using maltoheptaose (MH) as the hydrophilic group and PCL as the hydrophobic group to evaluate the influence of molecular weight and branching structures on self-assembled formations (**Fig. 7**).[159] The D_h obtained by DLS and morphology observed by TEM are summarized in the following table. A comparison of MH-*b*-PCL_{10k}, MH-*b*-$(PCL_{5k})_2$, and MH-*b*-$(PCL_{3.3k})_3$, keeping the molecular weights of the hydrophilic and hydrophobic groups constant, enabled an analysis of the effect of hydrophobic group branching on self-assembly behavior. The D_h values of MH-*b*-PCL_{10k}, MH-*b*-$(PCL_{5k})_2$, and MH-*b*-$(PCL_{3.3k})_3$ were 86, 98,

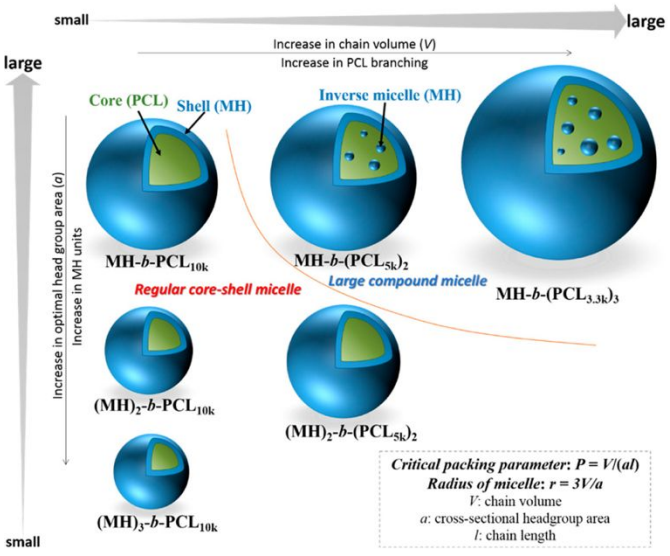

Fig. 7 Schematic illustration showing how the number of branches in the hydrophilic or hydrophobic chains of a miktoarm polymer affects micelle size. Reproduced with permission.[159] Copyright 2016, American Chemical Society.

and 112 nm, respectively, indicating that an increase in the branching structure of the hydrophobic groups resulted in a larger D_h. This was attributed to the observation that MH-*b*-PCL_{10k} formed spherical micelles, whereas MH-*b*-$(PCL_{5k})_2$ and MH-*b*-$(PCL_{3.3k})_3$ led to the formation of larger compound micelles, suggesting that the branched structure in the hydrophobic groups influenced the micelle morphology. The reasons for the morphological changes have been investigated. For example, the self-assembly behaviors of MH-*b*-PCL_{10k}, $(MH)_2$-*b*-PCL_{10k}, and $(MH)_3$-*b*-PCL_{10k} were compared as the number of hydrophilic group arms increased. The results showed that the micelle size decreased as the number of hydrophilic group arms increased, which can be explained by packing theory. Accordingly, the micelle radius (r) is given by $r = 3V/a$, where V represents the volume of the hydrophobic region and a symbolizes the cross-sectional area of the interface between hydrophilic and hydrophobic groups.[29] Considering that the molecular weights of the hydrophobic groups in MH-*b*-PCL_{10k}, $(MH)_2$-*b*-PCL_{10k}, and $(MH)_3$-*b*-PCL_{10k} are constant (V is constant), it is theoretically reasonable to conclude that an increase in the number of hydrophilic group arms increases the value of a, thereby decreasing the micelle radius.

This section discusses the morphological changes that occur in the self-assemblies formed by altering the molecular architectures of polymers from linear to miktoarm, as well as the causes of these changes. To clarify how increasing the number of hydrophobic arms impacts self-assembly behavior, Bae *et al.* synthesized linear polymers (PEG_m-*b*-$PLLA_{2n}$) and miktoarm polymers (PEG_m-*b*-$(PLLA_n)_2$) with hydrophilic group volume fractions (f_{PEG}) ranging from 0.2 to 0.7.[147] The linear polymers with f_{PEG} = 0.2 and 0.4 formed vesicles, while those with f_{PEG} = 0.6 and 0.7 formed spherical micelles. Conversely, all miktoarm polymers formed vesicles irrespective of the PEG volume fraction. Generally, amphiphilic block polymers with hydrophilic group volume fractions ranging from 0.2 to 0.4 are known to form vesicles. However, as the volume fraction of hydrophilic groups increases, the morphology of self-assembled structures transitions from vesicles to cylindrical and spherical micelles. Notably, the miktoarm polymers synthesized in this study formed vesicles across a broad range of hydrophilic group volume fractions (0.2–0.7), deviating from the behavior of simple linear polymers. Two perspectives are offered to elucidate this disparity in morphology despite comparable molecular weights of the hydrophilic and hydrophobic groups. First, the geometric structures of the polymer chains differ. The morphology of self-assembled amphiphilic polymers in aqueous solutions is typically dictated by the molecular weights of the hydrophilic and hydrophobic groups, as expounded by the CPP theory ($p = V/al$) proposed by Israelachvili *et al.*[29] In this study, both the linear and miktoarm polymers possess equal molecular weights for the hydrophilic and hydrophobic groups, meaning both polymers have equivalent a and V values. However, the l value of the miktoarm polymer is half that of the linear polymer, causing the miktoarm polymer's p to be larger than the linear polymer's p. Consequently, the miktoarm polymers can form vesicles over a broader range of hydrophilic group volume fractions compared with linear polymers. The second perspective is thermodynamic. The morphology of self-assembled structures is primarily influenced by the interactions among the free energies of three components: the stretching and contraction of the core-forming blocks, the interfacial free energy, and the corona interaction.[147] A miktoarm polymer with branched hydrophobic groups may induce greater crowding between adjacent hydrophobic groups and more stretching of the hydrophobic chains compared with a linear polymer, leading to the formation of vesicles even at higher volume fractions of hydrophilic groups (f_{PEG} = 0.6 and 0.7). Increasing the number of hydrophobic arms potentially reduces the curvature of the core-corona interface, supporting the formation of self-assembled structures with larger CPPs, such as fiber micelles and vesicles. In contrast, increasing the number of hydrophilic arms amplifies the curvature of the core-corona interface, transitioning the self-assembled structure to a smaller CPP morphology (**Fig. 8**).[160] Thus, curvature can be controlled by modulating the number of branches in amphiphilic miktoarm polymers, facilitating the formation of various self-assemblies, such as spherical micelles, rod-like micelles, and vesicles, with any hydrophilic-to-hydrophobic molecular weight composition ratio.

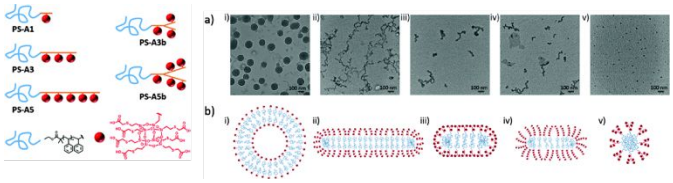

Fig. 8 Schematic illustration of linear and miktoarm polymers composed of PS and polyhedral oligomeric silsesquioxane (POSS), (a) TEM images of the micelles composed of amphiphilic linear and miktoarm polymers, and (b) schematic illustration of packing modes for linear and miktoarm polymers in micelles. Reproduced with permission.[160] Copyright 2016, Royal Society of Chemistry.

4. *Biomedical applications of self-assembled amphiphilic copolymers with different macromolecular architectures*

In previous sections, we examined the differences in self-assembly behavior between linear and nonlinear polymers. The findings indicate that the molecular architectures of these polymers significantly influence various properties, including the CMC, N_{agg}, D_h, and overall morphology of the resulting assemblies. In the subsequent sections, we demonstrate how alterations in the molecular architectures of polymers can enhance the performance of drug delivery carriers made from amphiphilic polymers, followed by an in-depth discussion on why materials derived from nonlinear polymers offer more effective functionalities compared with those derived from their linear counterparts.

4-1. *Applications of self-assemblies based on star polymers*

In this section, we first compare the performance of amphiphilic linear polymer aggregates with that of amphiphilic star-shaped polymer aggregates when used as drug delivery carriers. For example, Wang *et al.* synthesized a linear block polymer ($PCL_{4.7k}$-*b*-$PDMAEMA_{15k}$) and a 4-armed star polymer ($(PCL_{1.0k}$-*b*-$PDMAEMA_{3.8k})_4$) using PCL as the hydrophobic group and (PDMAEMA as the hydrophilic group.[139] The hydrophilic and hydrophobic groups of both polymers were synthesized to have comparable molecular weights, and the toxicity, doxorubicin (DOX) loading efficiency, and half-inhibitory concentration (IC_{50}) of DOX-loaded micelles obtained from each polymer were evaluated. The micelles derived from the 4-arm star polymers were less toxic to cells compared with those derived from linear block polymers. In addition, comparisons with previous reports showed that the 4-arm star polymer was less toxic than PDMAEMA-PCL-PDMAEMA triblock polymers with similar PDMAEMA molecular weights.[161] Micelles of the 4-arm star polymers exhibited higher DOX loading efficiencies (star: 16.6%, linear: 15.8%) and lower IC_{50} values compared with those of linear block polymers.

Furthermore, improved drug delivery performance was observed by increasing the number of arms in star polymers. Chen *et al.* synthesized amphiphilic star polymers with 4, 5, and 6 arms using PLLA as the hydrophobic block and tocopheryl polyethylene glycol 1000 succinate as the hydrophilic block.[162] They investigated the drug loading, entrapment efficiency, and release behavior of these polymers, revealing improvements in polymers with an increasing number of arms. This enhancement was attributed to stronger hydrophobic interactions within the micelle core and the incorporated drug, resulting from the formation of more compact micelles as the number of arms increased. This structure helped to reduce drug leakage and enabled a more controlled release. However, challenges were noted in micelles derived from star polymers, such as low drug loading capacity. Addressing this, Wang *et al.* developed a new 4-arm star amphiphilic polymer, incorporating poly(2-hydroxyethyl methacrylate) as the hydrophilic group, poly[2-(diethylamino)ethyl methacrylate] (PDEAEMA) as the hydrophobic group, and tetraphenylsilane (TPS) at the core. TPS was selected for its capacity to enhance nanomicelle formation and stability, support the 4 polymer arms, and facilitate π-π interactions with DOX. This design significantly increased the DOX loading capacity and efficiency.[163]

Several strategies are being explored beyond the incorporation of aromatic rings into the polymer backbone to improve the performance of polymer aggregates as drug delivery carriers. One approach is to encapsulate drugs in unimolecular micelles. Jayakannan *et al.* sought to characterize the efficacy of unimolecular micelles as drug carriers by synthesizing star polymers with varying numbers of arms (**Fig. 9**).[164] Their results suggest that unimolecular micelles are promising materials for next-generation drug delivery systems, demonstrating enhanced drug-carrying capacity, reduced drug leakage, and increased cellular uptake compared with aggregated micelles. In summary, several advances in the design of star polymers, such as aromatic ring inclusion and the use of unimolecular micelles, have significantly enhanced their applicability and efficiency in drug delivery systems.

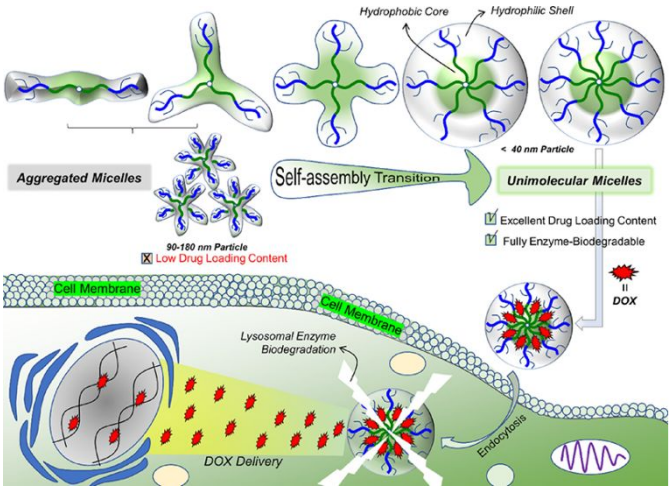

Fig. 9 Schematic illustration of anticancer activity of unimolecular micelles synthesized from star polymers with varying numbers of arms. Reproduced with permission.[164] Copyright 2023, American Chemical Society.

4-2. *Applications of self-assemblied cyclic polymers in drug delivery*

The influence of polymer molecular weight and structure on blood circulation is well known. Polymers with smaller molecular weights and sizes can penetrate the nanoporous structures of the kidneys, resulting in their elimination from the body. Studies by Szoka *et al.* have shown that cyclic comb polymers exhibit enhanced blood retention and uptake in cancer tumors compared with their linear counterparts.[165, 166] This can be attributed to the bulkier nature of the cyclic comb polymers, which requires the simultaneous permeation of two comb segments when penetrating the nanoporous kidney structures. In another example, O'Reilly *et al.* demonstrated that self-assemblies made from cyclic-linear graft copolymers exhibit significantly higher stability compared with those made from linear-linear graft copolymers. A notable feature of these cyclic-linear assemblies is their ability to disassemble upon the cleavage of a single bond in the cyclic polymer backbone, specifically through disulfide reduction in the presence of intracellular levels of L-glutathione. This property was leveraged to showcase the first instance of topology-controlled particle disassembly for the controlled release of an anticancer drug *in vitro*.[167] This demonstrates that the change in polymer architecture can be used as a trigger mechanism in the design of drug delivery vehicles. Liu *et al.* and Wei *et al.* explored polymers with different topologies, including amphiphilic tadpole polymers with cyclic structures, which demonstrated useful drug loading and release capacities.[111, 113] Notably, polymers with multiple cyclic structures exhibited improved performance metrics, such as reduced CMCs, increased drug

loading capacities, and improved cellular uptake efficiencies, in anticancer drug delivery applications. Further advances have been made in the synthesis of polymers that are responsive to pH variations, demonstrating improved therapeutic efficacy in cancer treatment. In addition, dual-responsive cyclic graft polymers have been developed that exhibit improvements in various parameters, such as micelle stability, drug loading, and cellular internalization efficiency under the influence of UV irradiation, demonstrating the potential of topological transformations for enhancing the anticancer activities of micelles (**Fig. 10**).[168] These groundbreaking developments underscore the untapped ability and versatility of cyclic polymers in advanced drug delivery technologies, providing opportunities for improved therapeutic strategies in cancer treatment.

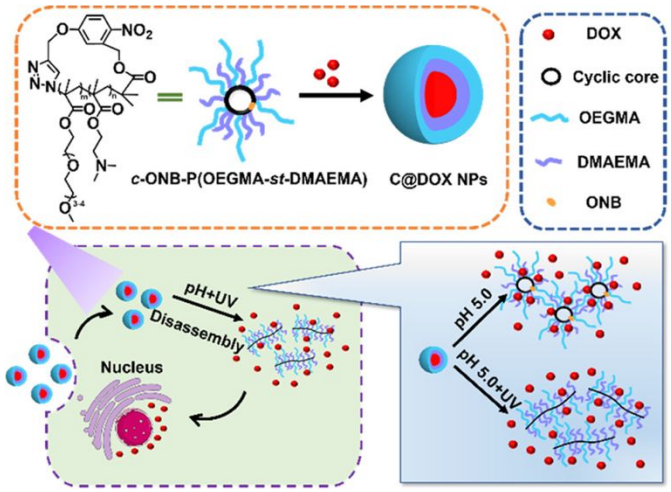

Fig. 10 Schematic illustration of micelles designed based on the topological transformation of dual-responsive cyclic graft copolymers to enhance anticancer activity. Reproduced with permission.[168] Copyright 2023, American Chemical Society.

5. Conclusions and Perspective

The macromolecular architecture of amphiphilic polymers is a key factor influencing their self-assembly behavior. The elucidation of this fact is a significant achievement, resulting from recent advances in polymer syntheses and structural analyses. However, the detailed mechanisms by which the macromolecular architecture induces variations in the self-assembly behavior have not been completely clarified. It is necessary to elucidate how macromolecular architectures affect self-assembly behavior and clarify the underlying mechanisms because these polymers have the potential to surpass existing polymeric materials based on linear block copolymers. This review aims to improve the understanding of these mechanisms by comparing the self-assembly behavior of amphiphilic linear polymers with systematically modified nonlinear polymers.

First, we present the typical synthesis strategies for ABA, star, and cyclic polymers and discuss the advantages and disadvantages of each approach. Then, we compare the self-assembly behavior of AB diblock copolymers with ABA, BAB, cyclic, and star polymers that have similar hydrophilic-to-hydrophobic molecular weight composition ratios, focusing on aspects such as CMC, D_h, N_{agg}, and morphology. We also investigate how differences in polymer structure affect self-assembly behavior from the thermodynamic and geometric perspectives. The findings show that polymer structure is closely related to the energy state during micellization, the curvature of the core-corona interface, and the packing parameters. Thus, this review helps bridge the gap between the influence of polymer structure on self-assembly behavior and the underlying mechanisms. In subsequent sections, we present applications of star-shaped and cyclic structures as drug delivery carriers and explain that self-assemblies derived from cyclic or star-shaped polymers exhibit greater stability and drug uptake capacity than those derived from linear polymers. Furthermore, we show that exploiting topological differences can enhance therapeutic efficacy. Therefore, designing polymers that exploit these topological differences may be an effective strategy for developing novel materials.

However, several areas remain to be addressed in future work. One such area is the combination of different types of polymers with different structures, including stimuli-responsive, rigid, and chiral polymers. For example, combining star or graft polymers with stimuli-responsive polymers may be a promising approach. The number and length of the arms in star polymers can be controlled to modulate stimuli-responsiveness. Similarly, controlling the spacing, degree of modification, or molecular weight of side-chain polymers in graft polymers may enable precise control of stimuli-responsiveness. Non-linear type polymers can be modified with different stimuli-responsive polymers. As a result, new polymeric materials that are responsive to different stimuli and capable of modifying their properties can be developed. Moreover, the relationship between the stiffness (persistence length) of polymer chains[169, 170] and the self-assembly behavior of nonlinear polymers needs to be explored.

Overall, this review presents examples where different polymer structures, particularly those with identical hydrophilic and hydrophobic molecular weight composition ratios, result in different morphologies of self-assemblies. This occurs because changes in polymer structure affect the packing style of the polymer chains, thereby affecting the packing parameters. If we can control the packing style of polymer chains, it may be possible to freely control packing parameters and create desired morphologies in nonlinear polymers. We believe it is necessary to study the effect of polymer chain stiffness on the self-assembly behavior of nonlinear polymers as a method to control the packing style. Varying the flexibility of the polymer chains may lead to reproducible changes in packing styles. In addition, the influence of block position and arrangement (such as in linear alternating copolymers or gradient polymers) on the self-assembly behavior of nonlinear polymers remains unexplored. Resolving the relationship between molecular architecture and polymer self-assembly is expected to promote the development of advanced polymer materials.

Abbreviations

MPEO Monomethoxy poly(ethylene oxide)
PS Poly(styrene)
CuAAC Copper-catalyzed azide-alkyne cycloaddition
RAFT Reversible addition-fragmentation chain transfer
CMC Critical micelle concentration
N_{agg} Aggregation number
D_h Hydrodynamic diameter
$f_{hydrophilic}$ Molecular weight composition of hydrophilic groups
PDMAEMA Poly[*N*, *N*-(dimethylamino)ethyl methacrylate]
PEO Poly(ethylene oxide)
PBO Poly(1,2-butylene oxide)
PCL Poly(caprolactone)
PBA Poly(*n*-butyl acrylate)
PMA Poly(methyl acrylate)
PNAM Poly(*N*-acryloylmorpholine)
SAXS Small-angle X-ray scattering
DLS Dynamic light scattering
PDMI Poly(dimethyl itaconate)
PPEGMA Poly[poly(ethylene glycol)methyl ether methacrylate]
CPP Critical packing parameter
TEM Transmission electron microscopy
PPO Poly(propylene oxide)
PISA Polymerization-induced self-assembly
PIB Poly[bis(isobutylene)]
PMeVE Poly[bis(methyl vinyl ether)]
PDMA Poly[2-(dimethylamino)ethyl methacrylate]
PDMS Poly(dimethylsiloxane)
HPMC Hydroxyl propyl methyl cellulose
PLLA Poly(L-lactide)
MH Maltoheptaose
DOX Doxorubicin
TPS Tetraphenylsilane

Author Contributions

The manuscript was written through contributions of all authors. All authors have given approval to the final version of the manuscript.

Conflicts of interest

There are no conflicts to declare.

Acknowledgements

This work was supported by the JSPS in the form of grants-in-aid for scientific research (B:22H02140, Exploratory:22K19057), and the MEXT Leading Initiative for Excellent Young Researchers, the JST FOREST Program (JPMJFR201P).

Notes and references

1. X. Zhu, Y. Zhou and D. Yan, *J. Polym. Sci. B: Polym. Phys.*, 2011, **49**, 1277-1286.
2. T.-P. Lin, A. B. Chang, S.-X. L. Luo, H.-Y. Chen, B. Lee and R. H. Grubbs, *ACS Nano*, 2017, **11**, 11632-11641.
3. M. Divandari, G. Morgese, L. Trachsel, M. Romio, E. S. Dehghani, J.-G. Rosenboom, C. Paradisi, M. Zenobi-Wong, S. N. Ramakrishna and E. M. Benetti, *Macromolecules*, 2017, **50**, 7760-7769.
4. F. M. Haque and S. M. Grayson, *Nat. Chem.*, 2020, **12**, 433-444.
5. C. Xu, C. He, N. Li, S. Yang, Y. Du, K. Matyjaszewski and X. Pan, *Nat. Commun.*, 2021, **12**, 5853.
6. L. Y. Qiu and Y. H. Bae, *Pharm. Res.*, 2006, **23**, 1-30.
7. M. Romio, L. Trachsel, G. Morgese, S. N. Ramakrishna, N. D. Spencer and E. M. Benetti, *ACS Macro Lett.*, 2020, **9**, 1024-1033.
8. W. Li, Y. Yu, M. Lamson, M. S. Silverstein, R. D. Tilton and K. Matyjaszewski, *Macromolecules*, 2012, **45**, 9419-9426.
9. W.-L. Chen, R. Cordero, H. Tran and C. K. Ober, *Macromolecules*, 2017, **50**, 4089-4113.
10. C. Feng, Y. Li, D. Yang, J. Hu, X. Zhang and X. Huang, *Chem. Soc. Rev.*, 2011, **40**, 1282-1295.
11. H. Dau, G. R. Jones, E. Tsogtgerel, D. Nguyen, A. Keyes, Y.-S. Liu, H. Rauf, E. Ordonez, V. Puchelle, H. Basbug Alhan, C. Zhao and E. Harth, *Chem. Rev.*, 2022, **122**, 14471-14553.
12. J. M. Ren, T. G. McKenzie, Q. Fu, E. H. H. Wong, J. Xu, Z. An, S. Shanmugam, T. P. Davis, C. Boyer and G. G. Qiao, *Chem. Rev.*, 2016, **116**, 6743-6836.
13. S. Ito, R. Goseki, T. Ishizone and A. Hirao, *Polym. Chem.*, 2014, **5**, 5523-5534.
14. A. B. Burns and R. A. Register, *Macromolecules*, 2016, **49**, 9521-9530.
15. L. Zhang, R. Elupula, S. M. Grayson and J. M. Torkelson, *Macromolecules*, 2016, **49**, 257-268.
16. F. S. Bates, *Science*, 1991, **251**, 898-905.
17. R. Adhikari and G. H. Michler, *Prog. Polym. Sci.*, 2004, **29**, 949-986.
18. J. Park, S. Jang and J. Kon Kim, *J. Polym. Sci. B: Polym. Phys.*, 2015, **53**, 1-21.
19. H. Feng, X. Lu, W. Wang, N.-G. Kang and J. W. Mays, *Journal*, 2017, **9**.
20. Y. Mai and A. Eisenberg, *Chem. Soc. Rev.*, 2012, **41**, 5969-5985.
21. M. Karayianni and S. Pispas, *J. Polym. Sci.*, 2021, **59**, 1874-1898.
22. J. Yun, R. Faust, L. S. Szilágyi, S. Kéki and M. Zsuga, *J. Macromol. Sci. A*, 2004, **41**, 613-627.
23. M. Qi and Y. Zhou, *Mater. Chem. Front.*, 2019, **3**, 1994-2009.
24. T. Yamamoto and Y. Tezuka, *Polym. Chem.*, 2011, **2**, 1930-1941.
25. H. Kono, M. Hibino, D. Ida, M. Ouchi and T. Terashima, *Macromolecules*, 2023, **56**, 6086-6098.
26. M. E. Fox, F. C. Szoka and J. M. J. Fréchet, *Acc. Chem. Res.*, 2009, **42**, 1141-1151.
27. N. P. Truong, M. R. Whittaker, C. W. Mak and T. P. Davis, *Expert Opin. Drug Deliv.*, 2015, **12**, 129-142.
28. M. J. Mitchell, M. M. Billingsley, R. M. Haley, M. E. Wechsler, N. A. Peppas and R. Langer, *Nat. Rev. Drug Discov.*, 2021, **20**, 101-124.
29. J. N. Israelachvili, D. J. Mitchell and B. W. Ninham, *J. Chem. Soc., Faraday Trans. 2*, 1976, **72**, 1525-1568.
30. R. J. Williams, A. P. Dove and R. K. O'Reilly, *Polym. Chem.*, 2015, **6**, 2998-3008.
31. D.-P. Yang, M. N. N. L. Oo, G. R. Deen, Z. Li and X. J. Loh, *Macromol. Rapid Commun.*, 2017, **38**, 1700410.
32. Y. Sakamoto and T. Nishimura, *Polym. Chem.*, 2022, **13**, 6343-6360.
33. E. Konishcheva, D. Daubian, J. Gaitzsch and W. Meier, *Helv. Chim. Acta*, 2018, **101**, e1700287.
34. A. O. Moughton, M. A. Hillmyer and T. P. Lodge, *Macromolecules*, 2012, **45**, 2-19.

35. X. Qiang, R. Chakroun, N. Janoszka and A. H. Gröschel, *Isr. J. Chem.*, 2019, **59**, 945-958.
36. J. Wan, B. Fan, K. Putera, J. Kim, M. M. Banaszak Holl and S. H. Thang, *ACS Nano*, 2021, **15**, 13721-13731.
37. X. He, L. Liang, K. Wang, S. Lin, D. Yan and Y. Zhang, *J. Appl. Polym. Sci.*, 2009, **111**, 560-565.
38. A. Debuigne, C. Detrembleur, C. Jérôme and T. Junkers, *Macromolecules*, 2013, **46**, 8922-8931.
39. Y. Nakamura, T. Arima, S. Tomita and S. Yamago, *J. Am. Chem. Soc.*, 2012, **134**, 5536-5539.
40. C. Li, Y. Tang, S. P. Armes, C. J. Morris, S. F. Rose, A. W. Lloyd and A. L. Lewis, *Biomacromolecules*, 2005, **6**, 994-999.
41. W. Zhu, W. Xie, X. Tong and Z. Shen, *Euro. Polym. J.*, 2007, **43**, 3522-3530.
42. W. Wu, W. Wang and J. Li, *Prog. Polym. Sci.*, 2015, **46**, 55-85.
43. K. Khanna, S. Varshney and A. Kakkar, *Polym. Chem.*, 2010, **1**, 1171-1185.
44. A. S. R. Oliveira, P. V. Mendonça, S. Simões, A. C. Serra and J. F. J. Coelho, *J. Polym. Sci.*, 2021, **59**, 211-229.
45. O. G. Schramm, G. M. Pavlov, H. P. van Erp, M. A. R. Meier, R. Hoogenboom and U. S. Schubert, *Macromolecules*, 2009, **42**, 1808-1816.
46. H. Gao and K. Matyjaszewski, *Macromolecules*, 2008, **41**, 1118-1125.
47. K. Ohno, B. Wong and D. M. Haddleton, *J. Polym. Sci., Part A: Polym. Chem.*, 2001, **39**, 2206-2214.
48. A. Blencowe, J. F. Tan, T. K. Goh and G. G. Qiao, *Polymer*, 2009, **50**, 5-32.
49. U. Tunca, Z. Ozyurek, T. Erdogan and G. Hizal, *J. Polym. Sci., Part A: Polym. Chem.*, 2004, **42**, 4228-4236.
50. M. Spiniello, A. Blencowe and G. G. Qiao, *J. Polym. Sci., Part A: Polym. Chem.*, 2008, **46**, 2422-2432.
51. A. Sulistio, A. Widjaya, A. Blencowe, X. Zhang and G. Qiao, *Chem. Commun.*, 2011, **47**, 1151-1153.
52. H. Gao and K. Matyjaszewski, *J. Am. Chem. Soc.*, 2007, **129**, 11828-11834.
53. H. Gao and K. Matyjaszewski, *Prog. Polym. Sci.*, 2009, **34**, 317-350.
54. X. Wei, G. Moad, B. W. Muir, E. Rizzardo, J. Rosselgong, W. Yang and S. H. Thang, *Macromol. Rapid Commun.*, 2014, **35**, 840-845.
55. J. M. Ren, Q. Fu, A. Blencowe and G. G. Qiao, *ACS Macro Lett.*, 2012, **1**, 681-686.
56. B. Zhang, H. Zhang, R. Elupula, A. M. Alb and S. M. Grayson, *Macromol. Rapid Commun.*, 2014, **35**, 146-151.
57. W. Yuan, J. Zhang, J. Wei, C. Zhang and J. Ren, *Euro. Polym. J.*, 2011, **47**, 949-958.
58. A. Dag, H. Durmaz, V. Kirmizi, G. Hizal and U. Tunca, *Polym. Chem.*, 2010, **1**, 621-623.
59. T. Josse, J. De Winter, P. Gerbaux and O. Coulembier, *Angew. Chem., Int. Ed.*, 2016, **55**, 13944-13958.
60. R. Liénard, J. De Winter and O. Coulembier, *J. Polym. Sci.*, 2020, **58**, 1481-1502.
61. Y. A. Chang and R. M. Waymouth, *J. Polym. Sci., Part A: Polym. Chem.*, 2017, **55**, 2892-2902.
62. Y. Tezuka and H. Oike, *Macromol. Symp.*, 2000, **161**, 159-168.
63. M. Kubo, T. Hayashi, H. Kobayashi, K. Tsuboi and T. Itoh, *Macromolecules*, 1997, **30**, 2805-2807.
64. D. Geiser and H. Höcker, *Macromolecules*, 1980, **13**, 653-656.
65. B. A. Laurent and S. M. Grayson, *Chem. Soc. Rev.*, 2009, **38**, 2202-2213.
66. B. A. Laurent and S. M. Grayson, *J. Am. Chem. Soc.*, 2006, **128**, 4238-4239.
67. J.-F. Lutz, *Angew. Chem., Int. Ed.*, 2007, **46**, 1018-1025.
68. M. D. Hossain, D. Valade, Z. Jia and M. J. Monteiro, *Polym. Chem.*, 2012, **3**, 2986-2995.
69. M. A. Cortez, W. T. Godbey, Y. Fang, M. E. Payne, B. J. Cafferty, K. A. Kosakowska and S. M. Grayson, *J. Am. Chem. Soc.*, 2015, **137**, 6541-6549.
70. J. N. Hoskins and S. M. Grayson, *Macromolecules*, 2009, **42**, 6406-6413.
71. D. M. Eugene and S. M. Grayson, *Macromolecules*, 2008, **41**, 5082-5084.
72. A. Touris and N. Hadjichristidis, *Macromolecules*, 2011, **44**, 1969-1976.
73. C. W. Bielawski, D. Benitez and R. H. Grubbs, *Science*, 2002, **297**, 2041-2044.
74. Y. Xia, A. J. Boydston, Y. Yao, J. A. Kornfield, I. A. Gorodetskaya, H. W. Spiess and R. H. Grubbs, *J. Am. Chem. Soc.*, 2009, **131**, 2670-2677.
75. R. Tuba, *Pure Appl. Chem*., 2014, 86, 1685-1693.
76. S. A. Gonsales, T. Kubo, M. K. Flint, K. A. Abboud, B. S. Sumerlin and A. S. Veige, *J. Am. Chem. Soc.*, 2016, **138**, 4996-4999.
77. T. S. Stukenbroeker, D. Solis-Ibarra and R. M. Waymouth, *Macromolecules*, 2014, **47**, 8224-8230.
78. E. Piedra-Arroni, C. Ladavière, A. Amgoune and D. Bourissou, *J. Am. Chem. Soc.*, 2013, **135**, 13306-13309.
79. A. Bunha, P.-F. Cao, J. D. Mangadlao and R. C. Advincula, *React. Funct. Polym.*, 2014, **80**, 33-39.
80. A. Narumi, S. Hasegawa, R. Yanagisawa, M. Tomiyama, M. Yamada, W. H. Binder, M. Kikuchi and S. Kawaguchi, *React. Funct. Polym.*, 2016, **104**, 1-8.
81. Y.-W. Yang, N.-J. Deng, G.-E. Yu, Z.-K. Zhou, D. Attwood and C. Booth, *Langmuir*, 1995, **11**, 4703-4711.
82. G.-E. Yu, Y.-W. Yang, Z. Yang, D. Attwood, C. Booth and V. M. Nace, *Langmuir*, 1996, **12**, 3404-3412.
83. H. Altinok, G.-E. Yu, S. K. Nixon, P. A. Gorry, D. Attwood and C. Booth, *Langmuir*, 1997, **13**, 5837-5848.
84. C. Booth and D. Attwood, *Macromol. Rapid Commun.*, 2000, **21**, 501-527.
85. Z. Zhou and B. Chu, *Macromolecules*, 1994, **27**, 2025-2033.
86. S. Zamani and S. Khoee, *Polymer*, 2012, **53**, 5723-5736.
87. S. H. Kim and W. H. Jo, *Macromolecules*, 2001, **34**, 7210-7218.
88. X. Zhao, W. Liu, D. Chen, X. Lin and W. W. Lu, *Macromol. Chem. Phys.*, 2007, **208**, 1773-1781.
89. L. Song, H. Sun, X. Chen, X. Han and H. Liu, *Soft Matter*, 2015, **11**, 4830-4839.
90. Y. Yu, D. Hong, Z. Liu, F. Jia, Y. Zhou and C. Leng, *J. Polym. Res.*, 2013, **20**, 235.
91. N. P. Balsara, M. Tirrell and T. P. Lodge, *Macromolecules*, 1991, **24**, 1975-1986.
92. S. Honda, T. Yamamoto and Y. Tezuka, *J. Am. Chem. Soc.*, 2010, **132**, 10251-10253.
93. A. J. de Graaf, K. W. M. Boere, J. Kemmink, R. G. Fokkink, C. F. van Nostrum, D. T. S. Rijkers, J. van der Gucht, H. Wienk, M. Baldus, E. Mastrobattista, T. Vermonden and W. E. Hennink, *Langmuir*, 2011, **27**, 9843-9848.
94. A. N. Semenov, J. F. Joanny and A. R. Khokhlov, *Macromolecules*, 1995, **28**, 1066-1075.
95. C. Lang, J. A. LaNasa, N. Utomo, Y. Xu, M. J. Nelson, W. Song, M. A. Hickner, R. H. Colby, M. Kumar and R. J. Hickey, *Nat. Commun.*, 2019, **10**, 3855.
96. C. Lang, M. Kumar and R. J. Hickey, *Polym. Chem.*, 2020, **11**, 375-384.
97. G.-E. Yu, Z. Yang, D. Attwood, C. Price and C. Booth, *Macromolecules*, 1996, **29**, 8479-8486.
98. G.-E. Yu, C. A. Garrett, S.-M. Mai, H. Altinok, D. Attwood, C. Price and C. Booth, *Langmuir*, 1998, **14**, 2278-2285.
99. L. Gao, Z. Ji, Y. Zhao, Y. Cai, X. Li and Y. Tu, *ACS Macro Lett.*, 2019, **8**, 1564-1569.
100. B. Zhang, H. Zhang, Y. Li, J. N. Hoskins and S. M. Grayson, *ACS Macro Lett.*, 2013, **2**, 845-848.
101. S. Honda, T. Yamamoto and Y. Tezuka, *Nat. Commun.*, 2013, **4**, 1574.

102. K. Heo, Y. Y. Kim, Y. Kitazawa, M. Kim, K. S. Jin, T. Yamamoto and M. Ree, *ACS Macro Lett.*, 2014, **3**, 233-239.
103. E. Minatti, R. Borsali, M. Schappacher, A. Deffieux, V. Soldi, T. Narayanan and J.-L. Putaux, *Macromol. Rapid Commun.*, 2002, **23**, 978-982.
104. E. Minatti, P. Viville, R. Borsali, M. Schappacher, A. Deffieux and R. Lazzaroni, *Macromolecules*, 2003, **36**, 4125-4133.
105. J.-L. Putaux, E. Minatti, C. Lefebvre, R. Borsali, M. Schappacher and A. Deffieux, *Faraday Discuss.*, 2005, **128**, 163-178.
106. B. J. Ree, T. Satoh and T. Yamamoto, *Journal*, 2019, **11**.
107. R. J. Williams, A. Pitto-Barry, N. Kirby, A. P. Dove and R. K. O'Reilly, *Macromolecules*, 2016, **49**, 2802-2813.
108. B. J. Ree, Y. Satoh, K. S. Jin, T. Isono and T. Satoh, *Macromolecules*, 2022, **55**, 862-872.
109. X. Wang, L. Li, X. Ye and C. Wu, *Macromolecules*, 2014, **47**, 2487-2495.
110. Y. Satoh, H. Matsuno, T. Yamamoto, K. Tajima, T. Isono and T. Satoh, *Macromolecules*, 2017, **50**, 97-106.
111. Y. Wang, Z. Wu, Z. Ma, X. Tu, S. Zhao, B. Wang, L. Ma and H. Wei, *Polym. Chem.*, 2018, **9**, 2569-2573.
112. G. Kang, L. Sun, Y. Liu, C. Meng, W. Ma, B. Wang, L. Ma, C. Yu and H. Wei, *Langmuir*, 2019, **35**, 12509-12517.
113. G.-Y. Kang, W. Ma, M.-Z. Liu, H.-X. Luo, C.-Y. Yu and H. Wei, *Macromol. Rapid Commun.*, 2021, **42**, 2100298.
114. G. Kang, Y. Liu, L. Li, L. Sun, W. Ma, C. Meng, L. Ma, G. Zheng, C. Chang and H. Wei, *Chem. Commun.*, 2020, **56**, 3003-3006.
115. X. Wan, T. Liu and S. Liu, *Biomacromolecules*, 2011, **12**, 1146-1154.
116. Y. Tao and H. Zhao, *Polymer*, 2017, **122**, 52-59.
117. B. J. Ree, Y. Satoh, K. Sik Jin, T. Isono, W. Jong Kim, T. Kakuchi, T. Satoh and M. Ree, *NPG Asia Mater.*, 2017, **9**, e453-e453.
118. J. Xu, J. Ye and S. Liu, *Macromolecules*, 2007, **40**, 9103-9110.
119. J. Ye, J. Xu, J. Hu, X. Wang, G. Zhang, S. Liu and C. Wu, *Macromolecules*, 2008, **41**, 4416-4422.
120. S. H. Lahasky, X. Hu and D. Zhang, *ACS Macro Lett.*, 2012, **1**, 580-584.
121. B. Liu, H. Wang, L. Zhang, G. Yang, X. Liu and I. Kim, *Polym. Chem.*, 2013, **4**, 2428-2431.
122. X.-P. Qiu, F. Tanaka and F. M. Winnik, *Macromolecules*, 2007, **40**, 7069-7071.
123. Y. Satokawa, T. Shikata, F. Tanaka, X.-p. Qiu and F. M. Winnik, *Macromolecules*, 2009, **42**, 1400-1403.
124. X. An, Q. Tang, W. Zhu, K. Zhang and Y. Zhao, *Macromol. Rapid Commun.*, 2016, **37**, 980-986.
125. Z. Wu, H. Zhang, C. Liu and C. Hong, *Macromol. Rapid Commun.*, 2021, **42**, 2100136.
126. T. Yamamoto, Y. Masuda, Y. Tezuka, E. Korchagina and F. M. Winnik, *Langmuir*, 2022, **38**, 5033-5039.
127. H. Wada, Y. Kitazawa, S. Kuroki, Y. Tezuka and T. Yamamoto, *Langmuir*, 2015, **31**, 8739-8744.
128. K. H. Kim, G. H. Cui, H. J. Lim, J. Huh, C.-H. Ahn and W. H. Jo, *Macromol. Chem. Phys.*, 2004, **205**, 1684-1692.
129. H. J. Lim, H. Lee, K. H. Kim, J. Huh, C.-H. Ahn and J. W. Kim, *Colloid Polym. Sci.*, 2013, **291**, 1817-1827.
130. Q. Liu, C. Cai and C.-M. Dong, *J. Biomed. Mater. Res. A*, 2009, **88A**, 990-999.
131. J. Cao, A. Lu, C. Li, M. Cai, Y. Chen, S. Li and X. Luo, *Colloids Surf. B.*, 2013, **112**, 35-41.
132. K. E. Washington, R. N. Kularatne, J. Du, M. J. Gillings, J. C. Webb, N. C. Doan, M. C. Biewer and M. C. Stefan, *J. Polym. Sci., Part A: Polym. Chem.*, 2016, **54**, 3601-3608.
133. G. Ma, C. Zhang, L. Zhang, H. Sun, C. Song, C. Wang and D. Kong, *J. Mater. Sci.: Mater.*, 2015, **27**, 17.
134. I. Ali, F. Kareem, S. Rahim, S. Perveen, S. Ahmed, M. R. Shah and M. I. Malik, *React. Funct. Polym.*, 2020, **150**, 104553.
135. H. Hyun, J. S. Cho, B. S. Kim, J. W. Lee, M. S. Kim, G. Khang, K. Park and H. B. Lee, *J. Polym. Sci., Part A: Polym. Chem.*, 2008, **46**, 2084-2096.
136. M. R. Whittaker and M. J. Monteiro, *Langmuir*, 2006, **22**, 9746-9752.
137. A. M. Alhoranta, J. K. Lehtinen, A. O. Urtti, S. J. Butcher, V. O. Aseyev and H. J. Tenhu, *Biomacromolecules*, 2011, **12**, 3213-3222.
138. R. d'Arcy, A. Gennari, R. Donno and N. Tirelli, *Macromol. Rapid Commun.*, 2016, **37**, 1918-1925.
139. Y.-L. Lo, G.-J. Chen, T.-H. Feng, M.-H. Li and L.-F. Wang, *RSC Adv.*, 2014, **4**, 11089-11098.
140. V. Karmegam, S. S. Kuruppu, C. M. Udamulle Gedara, M. C. Biewer and M. C. Stefan, *J. Polym. Sci.*, 2021, **59**, 3040-3052.
141. M. R. Whittaker, C. N. Urbani and M. J. Monteiro, *J. Polym. Sci., Part A: Polym. Chem.*, 2008, **46**, 6346-6357.
142. K. Hu, J. Sarkar, J. Zheng, Y. H. M. Lim and A. Goto, *Macromol. Rapid Commun.*, 2020, **41**, 2000075.
143. N. Ozawa, J. H. Lee, I. Akiba and T. Nishimura, *Polym. Chem.*, 2023, **14**, 3834-3842.
144. G. Mellot, P. Beaunier, J.-M. Guigner, L. Bouteiller, J. Rieger and F. Stoffelbach, *Macromol. Rapid Commun.*, 2019, **40**, 1800315.
145. Y. Zhang, M. Cao, G. Han, T. Guo, T. Ying and W. Zhang, *Macromolecules*, 2018, **51**, 5440-5449.
146. Y. C. Bae and R. Faust, *Macromolecules*, 1998, **31**, 2480-2487.
147. H. Yin, S.-W. Kang and Y. H. Bae, *Macromolecules*, 2009, **42**, 7456-7464.
148. K. Yoon, H. C. Kang, L. Li, H. Cho, M.-K. Park, E. Lee, Y. H. Bae and K. M. Huh, *Polym. Chem.*, 2015, **6**, 531-542.
149. J. Yun, R. Faust, L. S. Szilágyi, S. Kéki and M. Zsuga, *Macromolecules*, 2003, **36**, 1717-1723.
150. J. Yang, D. Zhang, S. Jiang, J. Yang and J. Nie, *J. Colloid Interface Sci.*, 2010, **352**, 405-414.
151. G. Maglio, F. Nicodemi, C. Conte, R. Palumbo, P. Tirino, E. Panza, A. Ianaro, F. Ungaro and F. Quaglia, *Biomacromolecules*, 2011, **12**, 4221-4229.
152. S. Gibanel, J. Forcada, V. Heroguez, M. Schappacher and Y. Gnanou, *Macromolecules*, 2001, **34**, 4451-4458.
153. H. Liu, J. Xu, J. Jiang, J. Yin, R. Narain, Y. Cai and S. Liu, *J. Polym. Sci., Part A: Polym. Chem.*, 2007, **45**, 1446-1462.
154. S. Pispas, N. Hadjichristidis, I. Potemkin and A. Khokhlov, *Macromolecules*, 2000, **33**, 1741-1746.
155. T. Satoh, N. Nishikawa, D. Kawato, D. Suemasa, S. Jung, Y. Y. Kim, M. Ree and T. Kakuchi, *Polym. Chem.*, 2014, **5**, 588-599.
156. T. Aliferis and H. Iatrou, *Euro. Polym. J.*, 2008, **44**, 2412-2417.
157. J. Wang, M. Caceres, S. Li and A. Deratani, *Macromol. Chem. Phys.*, 2017, **218**, 1600558.
158. A. Lu, J. Wang, M. C. Najarro, S. Li and A. Deratani, *Carbohydr. Polym.*, 2019, **211**, 133-140.
159. T. Isono, K. Miyachi, Y. Satoh, R. Nakamura, Y. Zhang, I. Otsuka, K. Tajima, T. Kakuchi, R. Borsali and T. Satoh, *Macromolecules*, 2016, **49**, 4178-4194.
160. Y. Chu, W. Zhang, X. Lu, G. Mu, B. Zhang, Y. Li, S. Z. D. Cheng and T. Liu, *Chem. Commun.*, 2016, **52**, 8687-8690.
161. C. Zhu, S. Jung, S. Luo, F. Meng, X. Zhu, T. G. Park and Z. Zhong, *Biomaterials*, 2010, **31**, 2408-2416.
162. J. Chen, A. Ding, Y. Zhou, P. Chen, Y. Xu and W. Nie, *Colloid Polym. Sci.*, 2019, **297**, 1321-1330.
163. Y. Shang, L. Guo and Z. Wang, *Macromol. Chem. Phys.*, 2019, **220**, 1900248.
164. U. Pranav, M. Malhotra, S. Pathan and M. Jayakannan, *ACS Biomater. Sci. Eng.*, 2023, **9**, 743-759.

165. N. Nasongkla, B. Chen, N. Macaraeg, M. E. Fox, J. M. J. Fréchet and F. C. Szoka, *J. Am. Chem. Soc.*, 2009, **131**, 3842-3843.
166. B. Chen, K. Jerger, J. M. J. Fréchet and F. C. Szoka, *J Control. Release*, 2009, **140**, 203-209.
167. M. C. Arno, R. J. Williams, P. Bexis, A. Pitto-Barry, N. Kirby, A. P. Dove and R. K. O'Reilly, *Biomaterials*, 2018, **180**, 184-192.
168. H. Liu, Z. Guo, W. Ma, S. Li, D. Wang, Z. Zheng, Y. Liu, C.-Y. Yu and H. Wei, *ACS Macro Lett.*, 2023, **12**, 1025-1030.
169. T. Nishimura, S. Fujii, K. Sakurai, Y. Sasaki and K. Akiyoshi, *Macromolecules*, 2021, **54**, 7003-7009.
170. T. Nishimura, Y. Hatatani, M. Ando, Y. Sasaki and K. Akiyoshi, *Chem. Sci.*, 2022, **13**, 5243-5251.